ARTICLES
https://doi.org/10.1038/s41590-021-00979-1

nature immunology

Check for updates

Epigenetic scars of CD8+ T cell exhaustion persist after cure of chronic infection in humans

Kathleen B. Yates[1,2,3], Pierre Tonnerre[4,5], Genevieve E. Martin[6,7], Ulrike Gerdemann[1], Rose Al Abosy[1], Dawn E. Comstock[1,8], Sarah A. Weiss[1,8], David Wolski[4], Damien C. Tully[9,10], Raymond T. Chung[4], Todd M. Allen[9], Arthur Y. Kim[11], Sarah Fidler[12,13], Julie Fox[14,15], John Frater[6,16], Georg M. Lauer[4], W. Nicholas Haining[1,17,18] ✉ and Debattama R. Sen[1,2,18] ✉

T cell exhaustion is an induced state of dysfunction that arises in response to chronic infection and cancer. Exhausted CD8+ T cells acquire a distinct epigenetic state, but it is not known whether that chromatin landscape is fixed or plastic following the resolution of a chronic infection. Here we show that the epigenetic state of exhaustion is largely irreversible, even after curative therapy. Analysis of chromatin accessibility in HCV- and HIV-specific responses identifies a core epigenetic program of exhaustion in CD8+ T cells, which undergoes only limited remodeling before and after resolution of infection. Moreover, canonical features of exhaustion, including super-enhancers near the genes *TOX* and *HIF1A*, remain 'epigenetically scarred.' T cell exhaustion is therefore a conserved epigenetic state that becomes fixed and persists independent of chronic antigen stimulation and inflammation. Therapeutic efforts to reverse T cell exhaustion may require new approaches that increase the epigenetic plasticity of exhausted T cells.

CD8+ T cell exhaustion is a hallmark of chronic viral infection and cancer[1]. In mouse models of chronic viral infection, exhausted T cells acquire varied functional deficits along with a distinct transcriptional and epigenetic state[2–4]. However, whether similar epigenetic changes underlie T cell dysfunction in chronic infections in humans as well as the ultimate differentiation of these T cells after curative therapy remains unknown.

T cell exhaustion has been extensively studied in mice using strains of the lymphocytic choriomeningitis virus (LCMV) and is characterized by expression of co-inhibitory receptors, low effector cytokine production and poor viral control[5–8]. Similar deficits have been observed in human T cells responding to chronic viral infections such as human immunodeficiency virus (HIV) and hepatitis C virus (HCV)[9–13]. Only 20–30% of HCV infections resolve spontaneously due to a variety of viral mechanisms for immune evasion, including viral escape[14]. Importantly, viral escape from CD8+ T cell responses through the mutation of recognized HCV epitopes happens early in disease progression[13,15–17]. Nevertheless, HCV infection becomes chronic in most cases and ultimately induces CD8+ T cell exhaustion in HCV-specific T cells.

Recently developed direct-acting antiviral (DAA) therapies have been strikingly effective, curing HCV infection in over 95% of patients[18–20]. Previous work has demonstrated that a subset of virus-specific T cells persists long-term after curative therapy[21,22] but do not regain substantial effector function. However, the mechanisms underlying these continued functional deficits and whether the removal of chronic stimulation can fundamentally reprogram the exhausted state remains unknown.

Here we show that exhausted CD8+ T cells responding to HCV and HIV share a core regulatory program that is largely irreversible after cure of infection, leading to epigenetic 'scarring'. The establishment of this exhaustion-associated program largely depends on chronic antigen stimulation and not the inflammatory milieu. Consistent with this, HCV-specific responses to mutated viral epitopes retain less of the exhausted epigenetic signature despite continued exposure to the inflammatory milieu. We develop an algorithm to infer super-enhancer activity directly from chromatin accessibility and show that epigenetic scars include exhaustion-specific super-enhancers. Scarred super-enhancers are found near key transcription factors, including TOX and HIF-1α, and are retained within HCV-specific T cells upon long-term follow-up of patients post DAA therapy. The epigenetic inflexibility of CD8+ T cell responses to HCV has crucial implications for clinical efforts to reverse T cell exhaustion and generate protective memory responses to chronic infection.

Results

Distinct epigenetic changes define T cells in chronic HCV. To characterize epigenetic changes following chronic HCV infection, we isolated 10–80,000 antigen-specific CD8+ T cells responding

[1]Department of Pediatric Oncology, Dana-Farber Cancer Institute, Boston, MA, USA. [2]Center for Cancer Research, Massachusetts General Hospital, Harvard Medical School, Charlestown, MA, USA. [3]Broad Institute of MIT and Harvard, Cambridge, MA, USA. [4]Division of Gastroenterology, Liver Center, Massachusetts General Hospital, Boston, MA, USA. [5]Inserm U976, Institut de Recherche Saint-Louis, Paris, France. [6]Nuffield Department of Medicine, University of Oxford, Oxford, UK. [7]Department of Infectious Diseases, Central Clinical School, Monash University, Melbourne, Australia. [8]Division of Medical Sciences, Harvard Medical School, Boston, MA, USA. [9]Ragon Institute of MGH, MIT and Harvard, Cambridge, MA, USA. [10]Department of Infectious Disease Epidemiology, London School of Hygiene and Tropical Medicine, London, UK. [11]Division of Infectious Diseases, Massachusetts General Hospital, Boston, MA, USA. [12]Division of Medicine, Wright Fleming Institute, Imperial College, London, UK. [13]Imperial College National Institute for Health Research Biomedical Research Centre, London, UK. [14]Department of Genitourinary Medicine and Infectious Disease, Guy's and St Thomas' NHS Foundation Trust, London, UK. [15]King's College National Institute for Health Research Biomedical Research Centre, London, UK. [16]Oxford National Institute for Health Research Biomedical Research Centre, Oxford, UK. [17]Merck Research Laboratories, Boston, MA, USA. [18]These authors contributed equally: W. Nicholas Haining, Debattama R. Sen. ✉e-mail: nick.haining@merck.com; dsen@mgh.harvard.edu

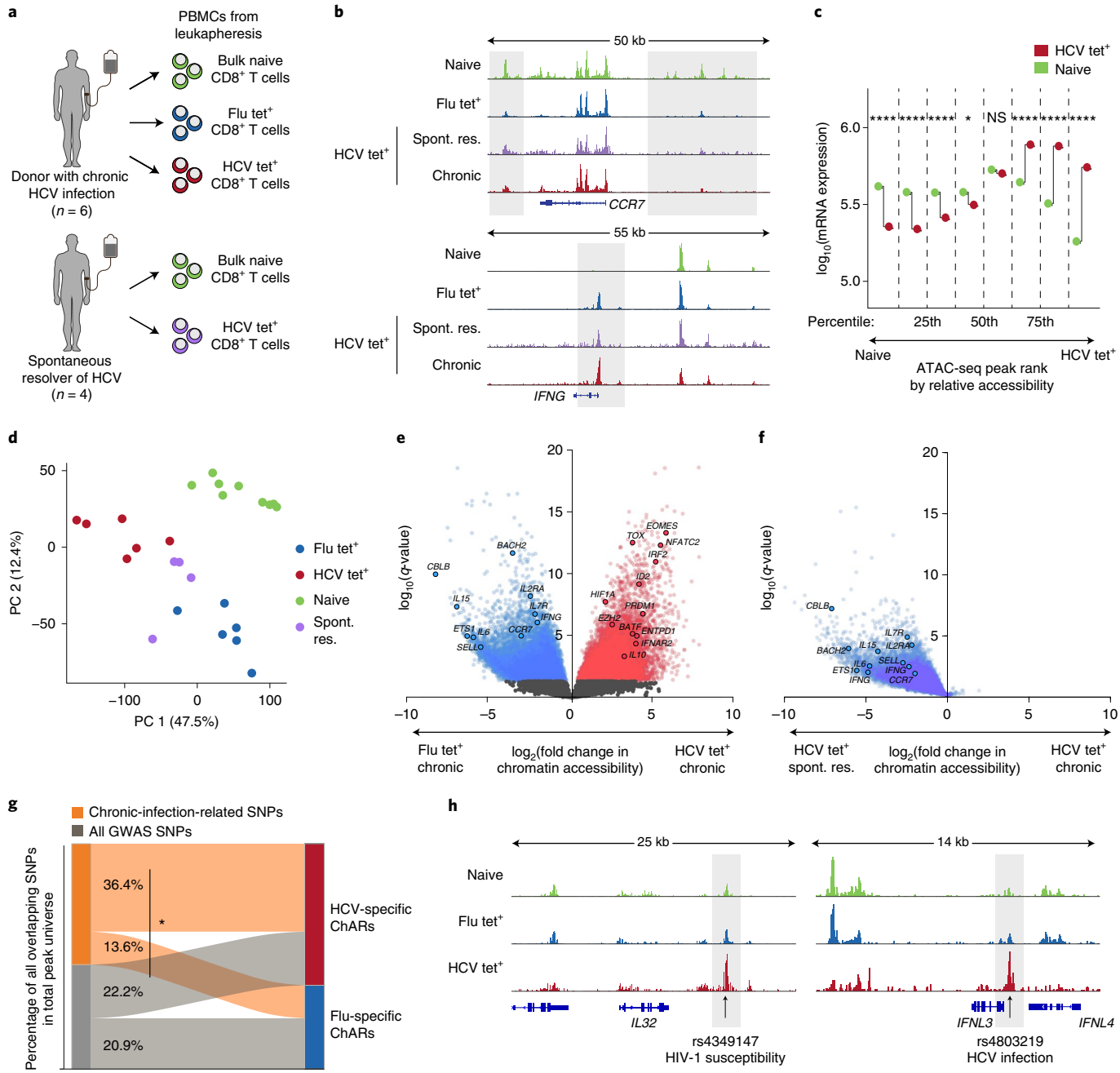

Fig. 1 | Distinct epigenetic changes underlie CD8⁺ T cell responses to Flu and chronic HCV infection. a, Schematic of the experiment. PBMCs, peripheral blood mononuclear cells. **b**, Representative ATAC-seq tracks at the *CCR7* and *IFNG* gene loci, with differential peaks highlighted in gray. **c**, Median mRNA expression levels of genes neighboring ChARs, which were partitioned into eight bins based on relative accessibility in naive versus HCV tet⁺ CD8⁺ T cells. **d**, Principal component (PC) analysis of naive, HCV tet⁺ and Flu tet⁺ CD8⁺ T cell populations from six patients. **e**, Volcano plot highlighting differential transcripts present in Flu tet⁺ CD8⁺ T cells versus HCV tet⁺ CD8⁺ T cells (colored dots, FDR < 0.05). **f**, Reprojection of Flu-specific ChARs from **e** onto volcano plots comparing HCV tet⁺ in spontaneously resolved (Spont. res.) versus chronic infection. **g**, Classification of SNPs within HCV- and Flu-specific ChARs. Single nucleotide polymorphisms that were subcategorized into those associated with chronic viral infection are summarized in Supplementary Table 3. **h**, Representative ATAC-seq tracks at the *IL32* and *IFNL3* gene loci, with the location of a SNP associated with HIV-1 susceptibility and with HCV infection, respectively, highlighted in gray. $^{*}P \leq 0.05$, $^{****}P \leq 0.0001$ and NS, not significant.

to HCV or influenza (Flu) virus—representing exhausted and functional memory responses, respectively—along with control naive CD8⁺ T cells from six donors with chronic HCV infection and four spontaneous resolvers of HCV infection (Fig. 1a, Extended Data Fig. 1a–c and Supplementary Table 1). We used assay for transposase-accessible chromatin using sequencing (ATAC-seq) to profile chromatin accessibility and identified 128,327 chromatin-accessible regions (ChARs) across all biological conditions (Supplementary Table 2). Marked enrichment of chromatin accessibility at transcriptional start sites and strong correlation between individual donor samples suggested high data quality (Extended Data Fig. 1d,e).

An initial inspection revealed chromatin accessibility changes consistent with the known biology of CD8⁺ T cells. As expected,

we observed increased accessibility at the *CCR7* gene locus in naive T cells, which encodes a key chemokine receptor expressed in that cell population (Fig. 1b). Conversely, antigen-experienced Flu- and HCV-specific T cells showed a gain of ChARs in the *IFNG* gene locus, consistent with upregulation of interferon (IFN)-γ in activated CD8$^+$ T cells (Fig. 1b). We then investigated how changes in chromatin accessibility relate to transcriptional differences between the populations. We ranked ChARs by differential accessibility and binned them into eight groups, ranging from most to least accessible in naive T cells relative to HCV tet$^+$ T cells from chronic infection. We observed significant and concordant changes in the average messenger RNA expression of neighboring genes in the top and bottom 25% of differential ChARs between naive and HCV-specific T cells ($P < 0.0001$; Mann–Whitney *U* test; Fig. 1c). The positive correlation between chromatin accessibility and mRNA transcription levels as well as strong enrichment for activating histone marks within ChARs suggested that the vast majority of differential ChARs act as positive regulators of gene expression (Extended Data Fig. 1f).

Principal component analysis (PCA) of all ChARs showed a clear separation of naive, Flu-specific and exhausted HCV-specific CD8$^+$ T cells (Fig. 1d). To characterize features that distinguished the Flu- and HCV-specific responses in chronic infection, we performed supervised differential accessibility analysis between Flu tet$^+$ and HCV tet$^+$ CD8$^+$ T cells. HCV tet$^+$ cells were found to have higher accessibility relative to Flu tet$^+$ cells in 21,490 regions (false-discovery rate (FDR) < 0.05; DESeq2), suggesting that the HCV-specific population had a markedly different chromatin accessibility landscape (Fig. 1e). Critically, the HCV tet$^+$ T cells from resolved infections were distinct from HCV tet$^+$ exhausted T cells from donors with a chronic infection by PCA projection, suggesting that disease specificity could not entirely explain the difference between HCV and Flu tet$^+$ T cells in chronic infection. Consistent with this, the HCV-specific population from the resolved infection group was more similar to Flu-specific T cells than exhausted HCV-specific T cells in chronic infection (Extended Data Fig. 1g). The majority of Flu-specific ChARs relative to HCV-specific ChARs in chronic infection were also more accessible in resolved HCV-specific responses (Fig. 1f). These data suggest that HCV-specific T cells in chronic settings have markedly different epigenetic changes compared with both donor-matched functional memory populations and resolved HCV infection. Differentially accessible ChARs in Flu- and resolved HCV-specific T cells were found near genes such as *IL15* and *IL7R*—important for CD8$^+$ T cell memory formation[23]—whereas chronic HCV-specific T cells had increased accessibility at loci including *EOMES*[3] and *NFATC2* (ref. [24]), which were previously implicated in regulating T cell exhaustion.

We then looked for evidence that these large-scale epigenetic changes were relevant in disease processes. We reasoned that if state-specific ChARs represented important regulatory units, they might be associated with disease-causing genetic variants, which are preferentially located in active promoters and enhancers relative to background noncoding regions. Given the known association between genetic variation and differences in chromatin accessibility—that is, ATAC quantitative trait loci[25]—we specifically focused on internally-controlled differences between Flu- and HCV-specific ChARs in donors with chronic infection and assayed the enrichment of single nucleotide polymorphisms (SNPs) derived from genome-wide association studies (GWAS). The HCV-specific ChARs tended to overlap SNPs at a greater rate per base pair compared with non-differential or Flu-specific ChARs (1.3-fold and 1.4-fold, respectively; Extended Data Fig. 1h). Furthermore, when subcategorized by etiology, SNPs related to chronic viral infections (Supplementary Table 3) were significantly overrepresented in the HCV-specific ChARs relative to Flu-specific ChARs (36.4 versus 13.6%; $P = 0.0042$, hypergeometric test; Fig. 1g). For example, a GWAS SNP for HIV-1 susceptibility was found within an HCV-specific ChAR near the *IL32* gene, which encodes a pro-inflammatory cytokine implicated in regulating disease outcome in chronic infection[26–29] (Fig. 1h). HCV-specific ChARs also overlapped at least one GWAS SNP found at the *IFNL3* locus, one of the strongest predictors of spontaneous viral clearance[30] (Fig. 1h). The exact role of these genes in chronic viral infections is still being investigated[30,31]. Nevertheless, these data suggest that the underlying mechanism of some GWAS SNP associations may be through modulation of enhancer activity in HCV-specific responses. Therefore, the CD8$^+$ T cell response to HCV involves large-scale differences in chromatin accessibility that are associated with regulatory activity in human disease.

Epigenetic signature of T cell exhaustion is conserved. We reasoned that the changes observed in HCV-specific T cells relative to Flu-specific T cells could be exhaustion-related or specific to the immunobiology of HCV. We therefore investigated whether the observed changes in chromatin accessibility could be recovered in the context of another chronic viral infection, HIV. A comparison of ATAC-seq profiles isolated from nine treatment-naive individuals infected with HIV identified 18,873 naive-specific and 22,978 HIV-specific ChARs (Fig. 2a,b, Extended Data Fig. 2a,b and Supplementary Table 4). As expected, the naive-specific ChARs identified in the individuals with an HIV infection were also more open in naive T cells isolated from the patients with HCV (Fig. 2c). Conversely, HIV-specific ChARs had greater accessibility on average in HCV tet$^+$ cells compared with their openness in naive and Flu tet$^+$ cells (Fig. 2c). Consistent with this, PCA separated not only naive T cells from antigen-experienced cells but also HIV- and HCV-specific T cells from Flu-specific memory T cells (Extended Data Fig. 2c). Shared greater accessibility was indeed observed in 12,637 ChARs within both HIV and HCV tet$^+$ cells relative to their naive T cell counterparts, representing a marked overlap ($P = 1 \times 10^{-5,338}$; hypergeometric test; Fig. 2d). All of the chronic-infection-related GWAS SNPs found within the HIV-specific ChARs were shared with the HCV-specific T cells, highlighting the potential functional role of this shared epigenetic profile. Thus, T cell exhaustion in human CD8$^+$ T cells induces hallmark epigenetic changes across multiple chronic viral infections such as HIV and HCV.

This shared regulatory program included HIV- and HCV-specific ChARs found near exhaustion-specific inhibitory receptor genes such as *ENTPD1* (encoding CD39; Fig. 2e). The HIV- and HCV-specific T cells also lacked memory-associated ChARs that were recovered near *CD127* (IL-7R) in the Flu tet$^+$ populations (Fig. 2e). Accordingly, Flu-specific ChARs enriched for pathways associated with IL-7 signaling and effector-memory formation, whereas HCV-specific ChARs were found near genes associated with NFAT signaling and PD-1 upregulation, both of which are related to T cell exhaustion (Fig. 2f).

Finally, we investigated whether chronic infection induces analogous changes in the CD8$^+$ T cell responses of mice and humans. We compared the Flu-, HCV- and HIV- specific epigenetic profiles with those of memory and exhausted CD8$^+$ T cells from acute and chronic infection in mice. The Flu tet$^+$ cells had higher accessibility in orthologous memory-specific regions defined in acute LCMV Armstrong ($P = 1.06 \times 10^{-60}$, hypergeometric test; Fig. 2g). Conversely, ChARs specific to HCV tet$^+$ and HIV tet$^+$ cells enriched for exhaustion-specific regions identified in chronic infection with LCMV Clone 13 ($P = 1.20 \times 10^{-83}$ and 6.25×10^{-6}, hypergeometric test; Fig. 2g). Exhaustion is therefore associated with an epigenetic state that is evolutionarily conserved between mouse and human chronic viral infections.

HCV-specific T cells retain epigenetic scars of exhaustion. Recently developed DAA therapies have enabled chronic HCV infection to be cured without the use of interferon[18–20]. However,

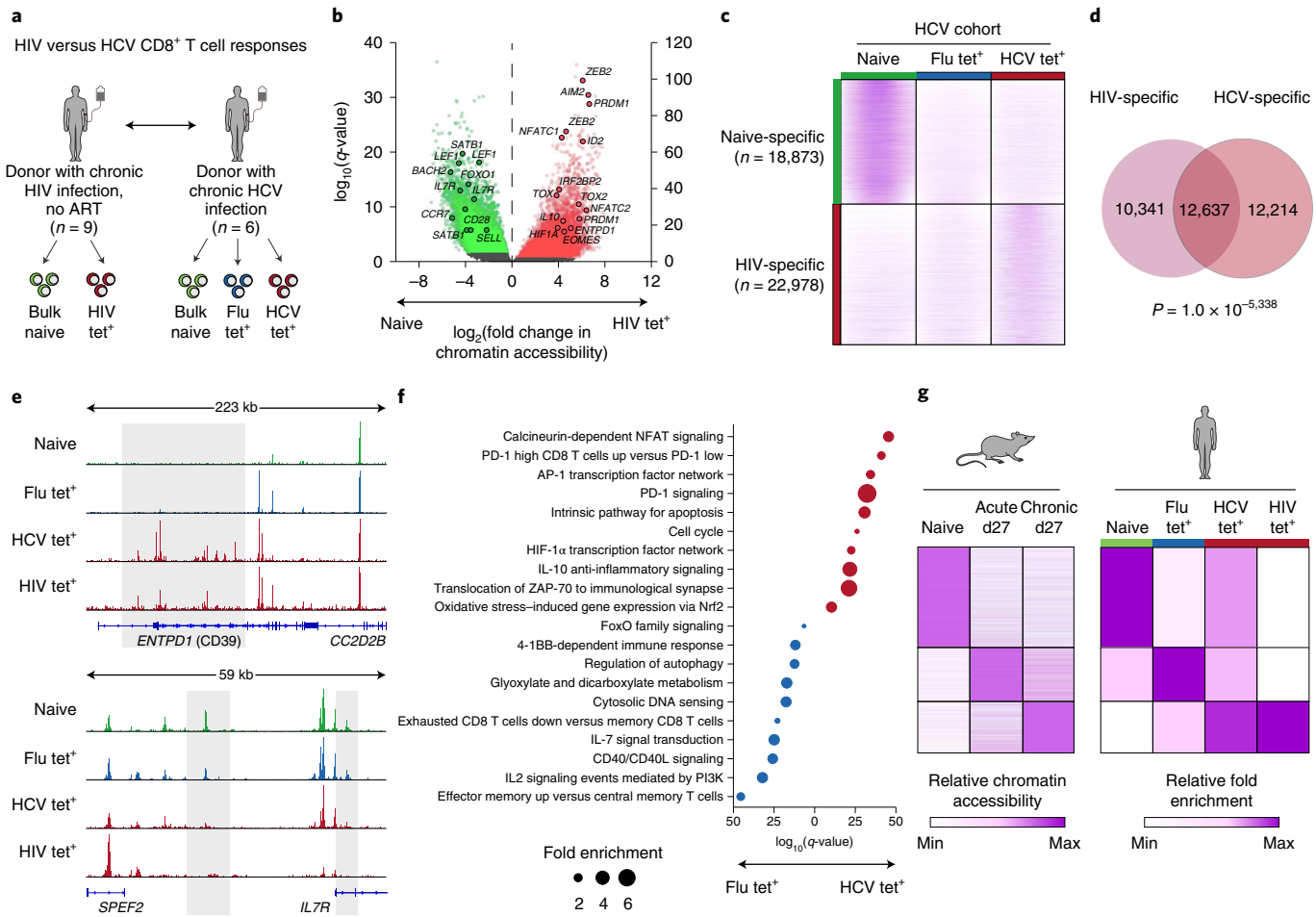

Fig. 2 | Epigenetic signature of T cell exhaustion is conserved across chronic viral infections. a, Schematic of the experiment. ART, antiretroviral therapy. **b**, Volcano plot highlighting differential transcripts present in HIV tet+ versus naive CD8+ T cells from patients with HIV (colored dots, FDR < 0.05). **c**, Chromatin accessibility at naive-specific and HIV-specific ChARs in the indicated conditions from the HCV cohort. **d**, Overlap between ChARs with increased accessibility in HIV and HCV tet+ T cells relative to naive T cells. **e**, Representative ATAC-seq tracks at the *ENTPD1* and *IL7R* gene loci, with differential peaks highlighted in gray. **f**, Gene ontology and gene-set enrichment (rows) in Flu- (blue) and HCV-specific (red) ChARs. The FDR values (hypergeometric test) are presented as $1-\log_{10}(q\text{-value})$. **g**, Heatmap of peak intensity within modules of ChARs (rows) from mouse naive CD8+ T cells and CD8+ T cells responding to acute and chronic LCMV (left). Fold enrichment of regions in human samples that are orthologous to naive, memory and exhaustion enhancers in mice (right). Min, minimum; max, maximum; and d27, day 27.

whether the removal of chronic antigen and inflammation can remodel the exhaustion-specific epigenetic program remains unknown. We investigated changes in the HCV tet+ population after cure of infection by profiling antigen-specific CD8+ T cells from the same donors 12 weeks after cessation of DAA therapy, which is approximately 20 weeks after viral clearance (Fig. 3a). A comparison of HCV tet+ cells before and after therapy indicated that 25,237 ChARs were differentially accessible (FDR < 0.05; DESeq2). Examples of differential ChARs that were lost following therapy included HCV tet+-specific ChARs near key exhaustion-associated genes such as *CTLA4* (Fig. 3b).

However, in addition to identifying instances of epigenetic remodeling, we identified exhaustion-specific ChARs that were not reversed (Fig. 3c,d). The ChARs near key genes such as *BATF* and *ENTPD1* remained accessible, consistent with the fact that high surface expression of CD39 was maintained following cure in the HCV tet+ population (Fig. 3c–e and Extended Data Fig. 3a). We analyzed ChARs genome-wide and found that ChARs specific to pre-treatment HCV tet+ cells could be broadly separated into two classes: those that were retained or 'scarred' and those that were 'reversed' by DAA therapy (Fig. 3f). We also studied ChARs that were 'gained' or became accessible in HCV tet+ cells only after the cure of infection (Fig. 3f). Pathway enrichment suggested that the scarred, reversed and gained ChARs regulated functionally distinct programs of genes (Fig. 3g). The scarred regions enriched for genes related to NFAT and HIF-1α signaling, whereas the reversed regions enriched for pathways such as translocation of ZAP-70 and PD-1 signaling. Shared enrichment of pathways including IL-7 signal transduction in Flu-specific as well as gained ChARs demonstrated that cure of infection could initiate some epigenetic changes associated with memory T cells.

We next investigated the regulatory impact of scarred versus reversed ChARs by assaying several associated features. We examined differential genomic localization and found that epigenetic scars were preferentially located in introns and intergenic regions (Extended Data Fig. 3b), suggesting an enrichment for distal regulatory elements. Scarred ChARs also had higher sequence conservation across mammals compared with the reversed regions (Fig. 3h), highlighting their potential importance. Scarred, but not reversed or gained ChARs, were enriched for GWAS SNPs related to chronic viral infections compared with all SNPs ($P = 0.021$, scarred; $P = 0.37$, reversed; and $P = 0.17$, gained; hypergeometric test; Extended Data

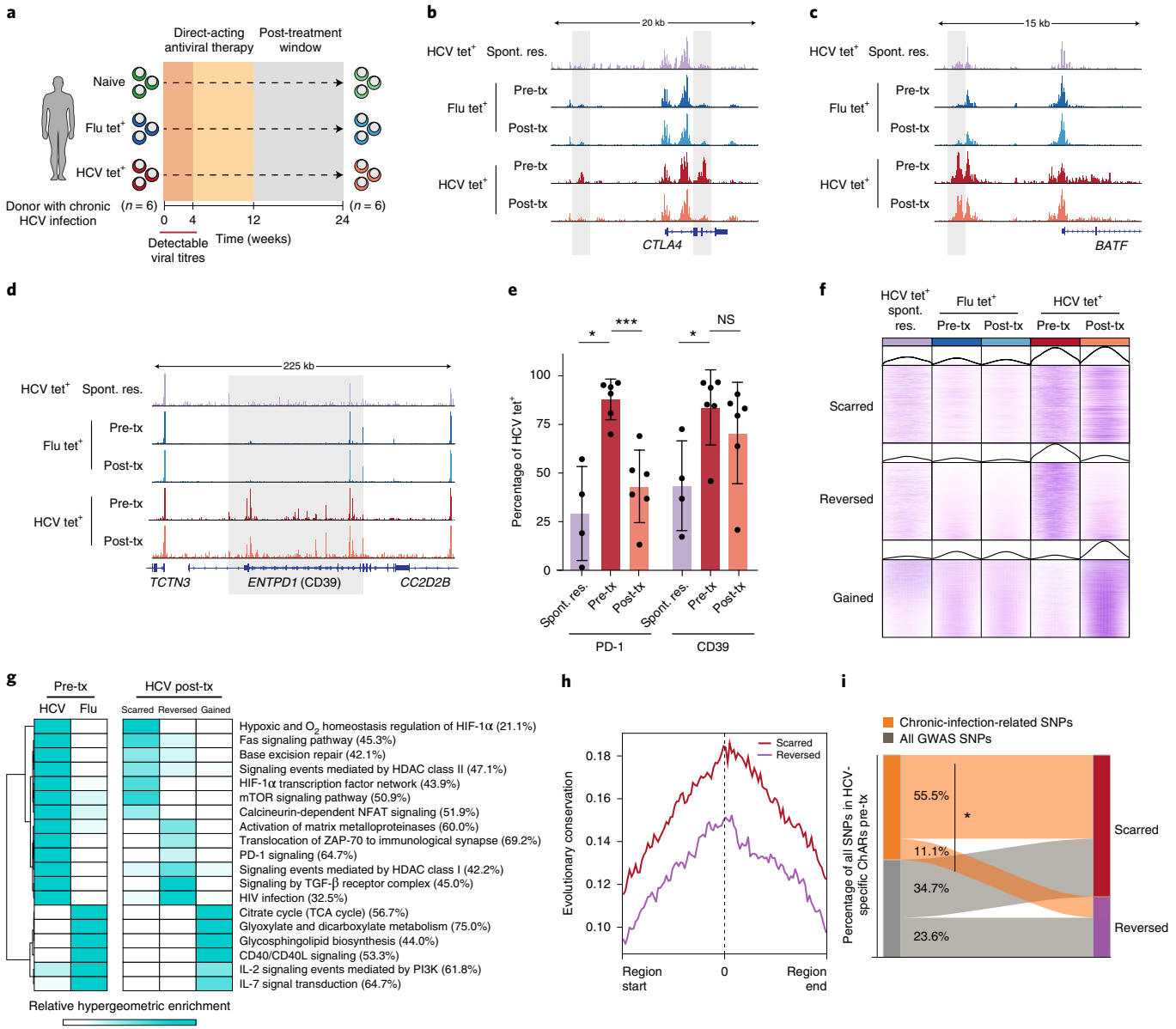

Fig. 3 | HCV-specific CD8⁺ T cells retain epigenetic scars of exhaustion despite cure of the chronic infection. a, Schematic of the treatment regimen. **b**–**d**, Representative ATAC-seq tracks at the *CTLA4* (**b**), *BATF* (**c**) and *ENTPD1* (**d**) gene loci, with differential peaks highlighted in gray. **e**, Frequency of PD-1 and CD39 in HCV-specific CD8⁺ T cells from spontaneously resolved and chronic HCV infection. Mean ± s.d. of $n = 6$ (chronic HCV) and 4 (resolved HCV infection) donors; two-sided Student's *t*-test with Welch's correction. **f**, Chromatin accessibility at scarred, reversed and gained ChARs in the indicated conditions from the HCV cohort. **g**, Heatmap showing pathway enrichment (rows) within HCV- and Flu-specific ChARs before treatment and within scarred, reversed and gained ChARs after treatment (columns). The percentage of overlapping genes observed within the total gene set is denoted in parentheses for the highest hypergeometric enrichment among scarred, reversed and gained regions. **h**, Average evolutionary conservation across the length of all ChARs within the scarred and reversed ChAR set. **i**, Alluvial diagram showing the chronic-infection-related SNPs and all SNPs from the GWAS that are shared between the HCV-specific ChARs before treatment, and the scarred and reversed ChARs post treatment. Spont. res., spontaneously resolved infection; tx, treatment; $^*P < 0.05$, $^{***}P < 0.001$ and NS, not significant.

Fig. 3c). The majority of HCV-specific ChARs that initially overlapped chronic-infection-related SNPs pre-DAA therapy were scarred rather than reversed post treatment (55.5 versus 11.1%; $P = 0.043$, hypergeometric test; Fig. 3i), suggesting that regions with the greatest regulatory impact in human disease were preferentially retained in exhausted T cells following cure.

Chronic TCR signaling is required for epigenetic scarring. Chronic antigen stimulation and persistent inflammation have each been thought to contribute to the development of T cell dysfunction[32]. We next investigated the relative contribution of these two factors in driving chromatin accessibility changes and the associated epigenetic scarring observed in chronic HCV-specific T cell responses.

We first examined the epigenetic changes induced by DAA therapy in bystander populations. Notably, almost no changes (<5 differential ChARs; FDR < 0.05) were detected in the naive and Flu-specific T cell populations before and after treatment (Fig. 4a). This finding could be explained in two ways: either T cell antigen receptor (TCR)-independent chronic inflammation does not mediate

significant epigenetic changes or those changes are permanent and thus unaffected by cure of infection. We reasoned that a comparison to naive and memory populations from uninfected donors could identify changes driven specifically by the inflammatory microenvironment in bystander populations. Therefore, we generated chromatin accessibility profiles from bulk naive and effector-memory populations from four healthy donors and compared them with the naive and bulk effector-memory T cells from patients infected with HCV (Fig. 4b). Less than 0.1% of all ChARs were differentially accessible between the respective naive and effector-memory populations in healthy donors versus HCV-infected donors (Fig. 4c). Furthermore, less than 5% of all ChARs were altered between the Flu-specific T cells in chronic HCV, which were marked by an effector-memory ($CCR7^{-}CD45RA^{-}$) phenotype (Extended Data Fig. 4a,b), and effector memory populations from healthy donors. In contrast, almost tenfold more ChARs (44,798 of 128,327; 34.9%) were differential between the Flu- and HCV-specific T cells. Consistent with this, naive and effector-memory responses (including Flu tet^{+} T cells) derived from donors with chronic infection co-clustered with their counterparts from healthy donors by PCA but were segregated from exhausted HCV-specific populations (Extended Data Fig. 4c). These data suggest that an inflammatory milieu imprints minimal epigenetic changes in bystander populations.

Chronic TCR stimulation is thought to be the other major contributor to the development of T cell exhaustion. To address this, we leveraged the presence of multiple HCV tet^{+} responses within each patient, including detected instances where the virus mutated away from the T cell epitope, thus abrogating or diminishing TCR signaling (escaped HCV responses, denoted 'HCV Esc'). We reasoned that a comparison of the previously characterized conserved HCV tet^{+} response to the HCV Esc tet^{+} response before DAA therapy would allow us to dissect the role of TCR signaling while controlling for the inflammatory milieu.

First, we examined the inhibitory receptor expression on antigen-specific $CD8^{+}$ T cell populations before and after infection resolution. We noted that the HCV Esc tet^{+} population had lower PD-1 expression than HCV tet^{+} cells before the initiation of DAA therapy (47 versus 87%; Fig. 4d and Extended Data Fig. 4d). Hierarchical clustering of samples before DAA therapy showed that the HCV Esc tet^{+} response was epigenetically more similar to the functional Flu tet^{+} response than the exhausted HCV tet^{+} response (Fig. 4e). This was supported by the fact that the HCV Esc-specific ChARs failed to enrich for mouse-model-derived signatures of exhaustion (Fig. 4f) and that the resolution of infection led to minimal differences in the HCV Esc tet^{+} response (<250 differential ChARs, FDR < 0.05). Together, these data suggest that epigenetic changes of exhaustion could not be solely attributed to the presence of inflammation and that chronic TCR stimulation might instead be a major driver.

Next, we investigated how the establishment of epigenetic scars might be affected by an early loss of TCR signaling in the context of chronic viral infection. A comparison of scarred ChARs between the HCV tet^{+} and HCV Esc tet^{+} responses revealed distinct patterns of accessibility (Fig. 4g). The scars shared between the HCV tet^{+} and HCV Esc tet^{+} cells were presumably acquired early in the course of infection. Accordingly, these ChARs were enriched for motifs of canonical transcription factors in exhaustion, such as T-bet and EOMES ($P < 0.05$, hypergeometric test). Importantly, the lack of a strong memory enrichment in the HCV Esc-specific responses (Fig. 4f) could probably be explained by the presence of these epigenetic scars and may underlie the lack of protective memory formation in chronic HCV as noted in previous studies[21,22]. Nevertheless, the majority of scarred ChARs were only observed in the HCV tet^{+}, but not in the HCV Esc tet^{+} responses, and were thus probably related to the chronicity of viral exposure. Consistent with this, these ChARs were enriched for motifs related to STATs and AP-1 family members, which are often activated downstream of TCR ligation (Fig. 4g). Early versus late scarred regions were also differentially enriched for pathways related to apoptosis, inhibitory receptor signaling and lipid metabolism (Extended Data Fig. 4e). These data are consistent with a model where the degree and duration of chronic TCR signaling, rather than the inflammatory microenvironment, drive epigenetic scarring in exhaustion.

Scars represent critical epigenetic hallmarks of exhaustion. We next investigated the impact of epigenetic scarring on the regulation of T cell exhaustion. Characterization of super-enhancers and their associated genes has been utilized to define important regulatory nodes in many cell types[33–36] but the evaluation of super-enhancer activity in exhausted T cells using standard H3K27 acetylation chromatin immunoprecipitation and sequencing (H3K27ac ChIP-seq) has been limited by low cell numbers. Therefore, we developed a method relying solely on chromatin accessibility profiles generated using ATAC-seq that allow the inference of super-enhancer activity and recapitulate H3K27ac ChIP-seq-based results. As expected, we saw concordant enrichment of H3K27ac signal and presence of open chromatin at the *ETS1* super-enhancer locus in $CD4^{+}$ T cells (Extended Data Fig. 5a)[36]. The chromatin accessibility data could largely predict H3K27ac-based super-enhancer identities across eight human cell types, with area-under-the-curve values ranging from 0.76 to 0.86 (Extended Data Fig. 5b). The super-enhancer-associated genes identified through ATAC-seq were transcribed at higher levels than the non-super-enhancer-associated genes in each respective cell type (Extended Data Fig. 5c), providing further support for our ability to accurately identify super-enhancer-associated genes solely from open chromatin regions[37].

Having validated our method for identifying super-enhancers, we then applied it to the epigenetic scars in HCV tet^{+} cells (Fig. 5a). The gene encoding the transcription factor TOX was ranked as the top super-enhancer-associated gene within the scarred regions (Fig. 5a,b). This is consistent with the known role of TOX as a critical regulator of exhausted T cells in multiple contexts of chronic stimulation[3,38–40]. Strikingly, *TOX* mRNA expression was elevated in pre-treatment HCV tet^{+} cells relative to both HCV Esc and spontaneously resolved HCV infection (Extended Data Fig. 5d), and was not altered by DAA therapy. Other super-enhancer-associated transcription factors included HIF-1α, ID2 and NFAT (Fig. 5a), along with others that may represent previously unknown regulators of the exhausted state.

As expected, the super-enhancer-associated genes had higher levels of mRNA expression than the non-super-enhancer genes in HCV-specific T cells (Fig. 5c). To explore the regulatory impact of super-enhancer-associated transcription factors, we performed differential motif enrichment between scarred and reversed ChARs. Strikingly, a large fraction of the super-enhancer-associated transcription factors had motifs that were overrepresented in the scarred regions compared with the reversed regions (Fig. 5d). This included HIF-1α as well as other exhaustion-associated transcription factors such as EOMES, RUNX1 and BATF. Importantly, these transcription factors are themselves differentially regulated by epigenetic scars. Therefore, the overrepresentation of their downstream binding sites in those same scars indicates the existence of a positive feedback loop that may reinforce the epigenetic state of T cell exhaustion. Consistent with this, the ChARs that were newly gained following DAA therapy were associated with significant changes in the average mRNA expression levels of the neighboring genes ($P = 0.0022$, paired Student's *t*-test), whereas the transcription of genes neighboring the scarred and reversed ChARs was unaltered (Fig. 5e). The continued elevated transcription of genes adjacent to the reversed ChARs further highlights the fixed differentiation state of HCV-specific T cells after infection resolution. Together, these data suggest that failure to reverse $CD8^{+}$ T cell exhaustion after curative therapy may be mediated by the activity of distinct transcriptional regulators within epigenetic scars.

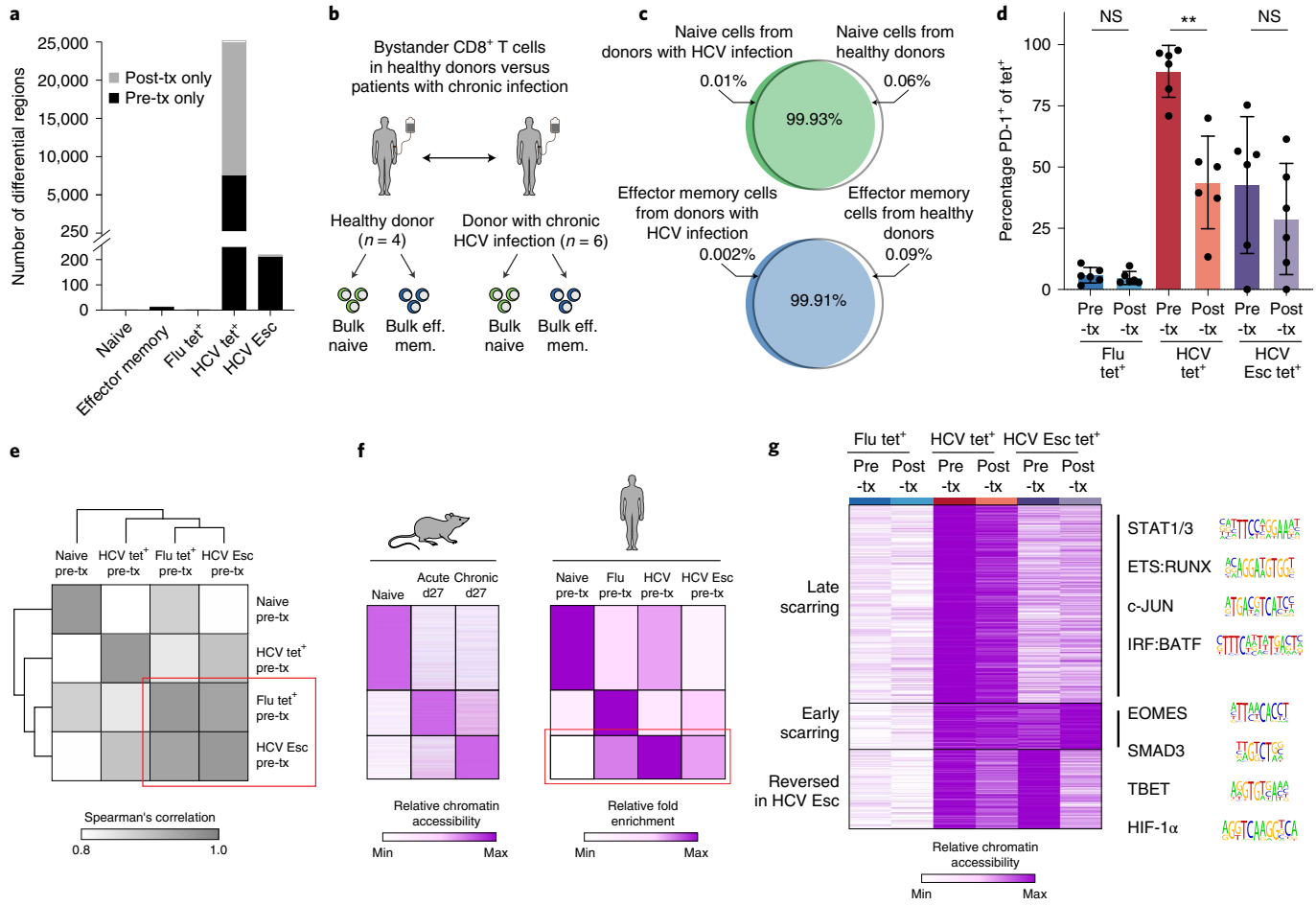

Fig. 4 | Chronic TCR signaling, and not the inflammatory milieu, drives epigenetic scarring in exhausted CD8⁺ T cells. a, Number of differential ChARs in the indicated conditions before and after DAA therapy. **b**, Schematic of the experiment. Eff. mem, effector memory. **c**, Overlap of ChARs in naive T cells (top) and bulk effector-memory cells from healthy donors and individuals with HCV infection. **d**, Frequency of PD-1 staining on tetramer populations before and after DAA therapy. Mean ± s.d. of $n = 6$ donors; two-sided Student's *t*-test with Welch's correction; $^{**}P \leq 0.01$ and NS, not significant. **e**, Clustered similarity matrix between the indicated biological conditions at the pre-treatment time point. The red rectangle highlights the similarity between Flu tet⁺ and HCV Esc T cells. **f**, Heatmap of the peak intensity within modules of ChARs (rows) from mouse naive CD8⁺ T cells and CD8⁺ T cells responding to acute and chronic LCMV at day 27 (d27; left). Fold enrichment in human samples of regions orthologous to mouse naive, memory and exhaustion enhancers (right). **g**, Heatmap of chromatin accessibility within scarred ChARs (rows) clustered across the indicated cell states (columns). Sequence logos for transcription factor motifs enriched in the indicated clusters (right). Min, minimum; max, maximum; and tx, treatment.

Epigenetic scars of exhaustion are retained long-term. Our results suggested that cure of infection through DAA therapy leaves epigenetic scars that include regions regulating the function of exhausted T cells. However, it is possible that these regions simply represent those that are slower to revert than others. To test this, we profiled four patients 60–80 weeks after cessation of therapy (Fig. 6a). The chromatin accessibility profiles of the HCV tet⁺ cells at this late time point largely clustered with those generated immediately following therapy as opposed to pre-treatment (Fig. 6b). We then compared the reversed ChARs at the late time point with the post-therapy measurement and found that about half were unchanged, whereas the rest continued to decrease in accessibility over time (Fig. 6c). In contrast, 77.1% of the scarred ChARs remained unchanged and only 18.2% diminished in accessibility in the long-term follow-up (Fig. 6c). The regions that remained accessible at this late time point included the super-enhancer near *TOX* (Fig. 6d). Overall, these data suggest that the epigenetic scars of exhaustion are retained long-term after cure of infection, probably restraining the formation of protective memory responses to HCV.

Discussion

T cell responses to chronic viral infections are characterized by a range of functional defects[10–12,41,42] but the epigenetic mechanisms that specify T cell exhaustion and the potential for reprogramming the exhausted cell state after curative therapy remains an open question. Here we show that the landscape of regulatory regions in HCV-specific exhausted CD8⁺ T cells is markedly different from memory responses, is established in a TCR-dependent fashion and becomes fixed despite cure of infection. HCV-specific epigenetic changes are conserved across chronic viral infection settings where T cell exhaustion is observed, including HIV and the LCMV mouse model. By developing an algorithm to infer super-enhancer activity despite low cell input, we also pinpoint key transcriptional regulators of exhaustion such as TOX and HIF-1α within these epigenetic scars. These findings have important implications for understanding the regulation of exhausted T cells at the epigenetic level.

First, we show that T cell exhaustion is defined by a distinct epigenetic program that is conserved across chronic viral infection paradigms, including HIV and the LCMV mouse model. Although this has been previously established in mouse models of chronic

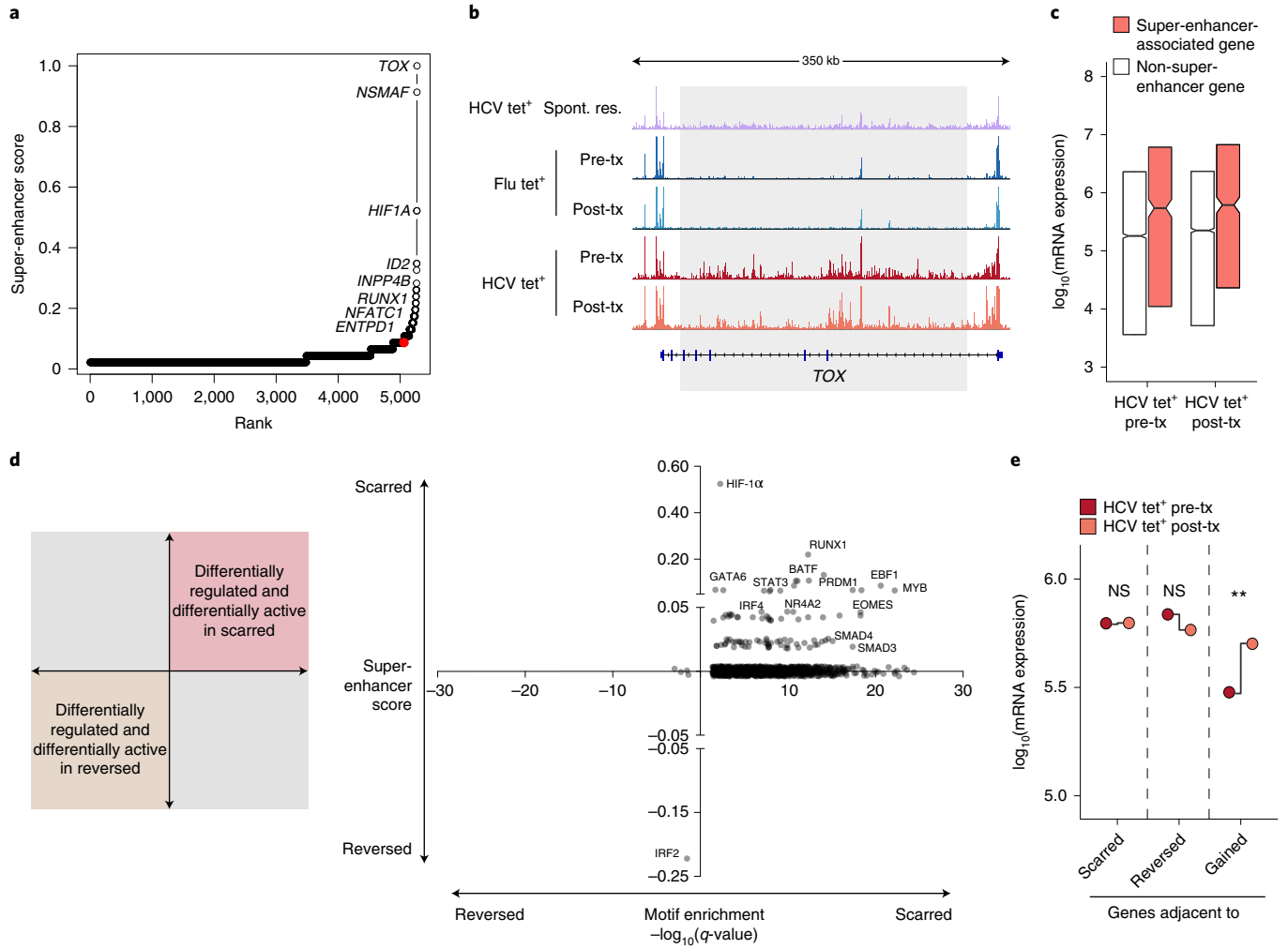

Fig. 5 | Scarred regions identify critical regulators of exhaustion. a, Super-enhancer elbow plots based on ChARs within the scarred set of regions. The red dot denotes the inflection point in the curve demarcating super-enhancers from other regions. **b**, Representative ATAC-seq tracks at the *TOX* gene locus, with differential peaks highlighted in gray. Spont. res., spontaneously resolved infection. **c**, Levels of mRNA expression in HCV tet$^+$ cells before and after treatment, partitioned according to genes with or without an associated super-enhancer. Center, median; box limits, first and third percentiles. **d**, Schematic (left) and plot (right) of transcription factors based on their super-enhancer ranking (*y* axis) and differential motif enrichment between scarred and reversed ChARs (*x* axis). Left schematic highlights the interpretation of double-positive and double-negative quadrants in the right plot. **e**, Median mRNA expression levels of genes neighboring scarred, reversed and gained ChARs. Gene expression from HCV tet$^+$ cells before and after treatment are shown. Two-sided paired Student's *t*-test, $^{**}P \leq 0.01$; NS, not significant; and tx, treatment.

viral infection[4,43,44], previous studies in humans have been limited by the small numbers of virus-specific T cells that can be isolated from patients. Here we overcame this by analyzing leukapheresis samples from a specifically designed interventional trial to investigate the fate of exhausted HCV-specific T cells and further compare them to treatment-naive HIV samples. We show that antigen-specific exhausted T cells in multiple human viral infections adopt a similar epigenetic profile in response to chronic stimulation. By mapping chromatin accessibility changes in several contexts of T cell exhaustion, we also establish a core epigenetic signature that can act as a biomarker of the exhausted state in human CD8$^+$ T cells.

Second, we dissect the relative contribution of chronic TCR signaling versus the inflammatory milieu in driving epigenetic changes. Previous studies in both mice and humans have highlighted the potential role of chronic type I IFN signaling as well as the role of immunosuppressive cytokines such as IL-10 and TGF-β in the development of T cell exhaustion[45–48]. Separating direct cell-intrinsic effects in CD8$^+$ T cells from indirect effects mediated by other populations remains a challenge in these studies. We resolve this by studying the antigen-specific responses to acute and chronic viral infections within the same patient, thereby controlling for microenvironment effects. We show that the epigenetic profile of the effector-memory-phenotype Flu-specific T cells and bulk effector-memory populations in chronic infection are virtually indistinguishable from that of effector-memory cells from healthy donors. Furthermore, we observe partial epigenetic remodeling within HCV-specific responses where viral epitope escape has abrogated specific TCR recognition despite continued exposure to the inflammatory milieu. These data suggest that chronic TCR signaling, rather than the inflammatory microenvironment, is largely responsible for inducing epigenetic changes associated with T cell exhaustion.

Third, we find only limited remodeling of the epigenetic landscape after cure of infection, suggesting that the exhausted T cell state cannot be fully reversed with DAA treatment. Epigenetic scars are indeed preserved for over a year after termination of viremia and removal of chronic antigen. The scarred regions are enriched for disease-associated SNPs relative to reversed regions following DAA therapy, suggesting they may have a greater regulatory role

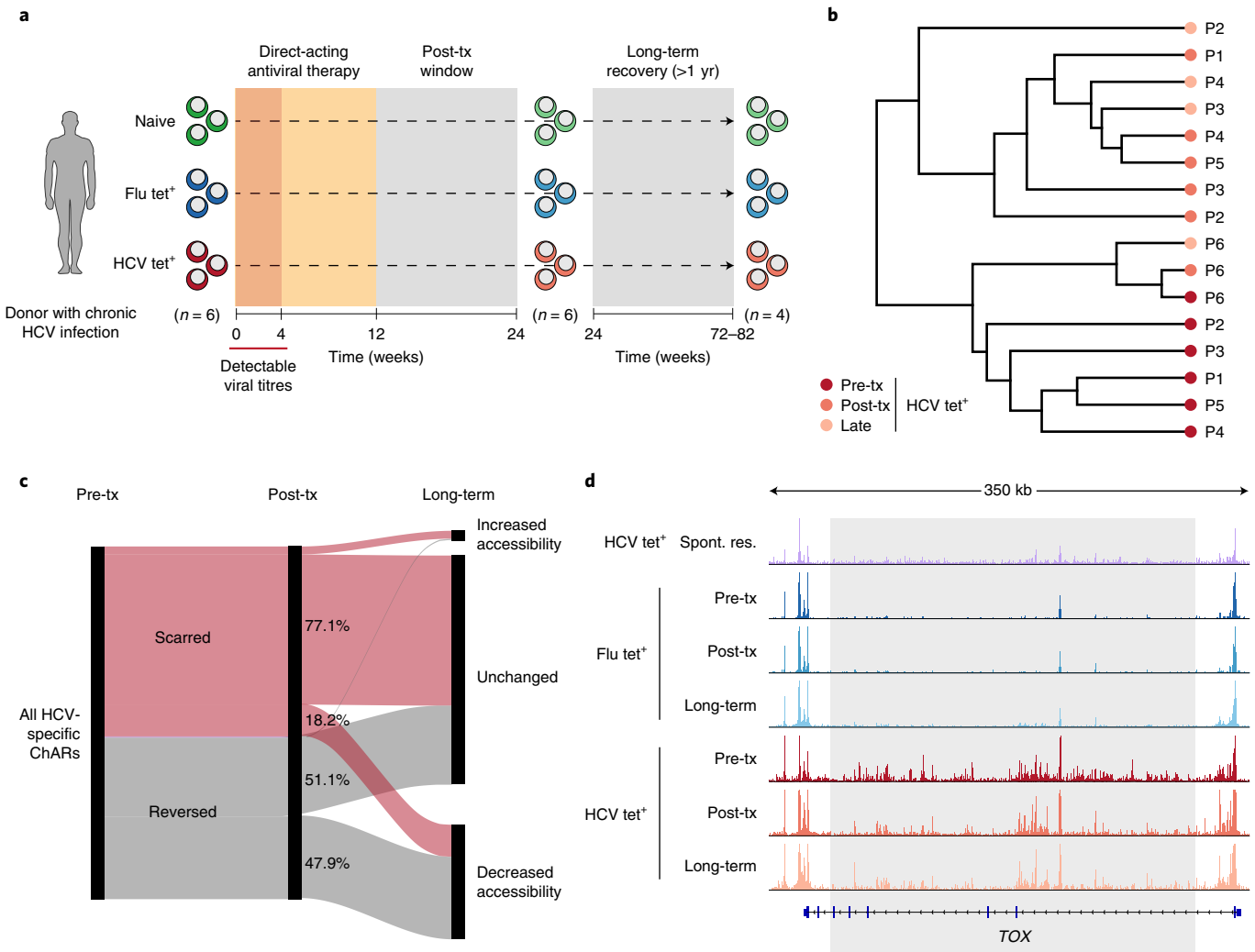

Fig. 6 | Epigenetic scars of exhaustion are retained long-term following infection cure. a, Schematic of the experimental time points before and after DAA therapy. **b**, Clustering of individual HCV tet+ profiles from patients (P1–P6) across three time points (pre-treatment, post treatment and long-term follow-up post treatment (late)). **c**, Longitudinal trajectory of scarred and reversed ChARs at each time point. **d**, Representative ATAC-seq tracks at the *TOX* gene locus, with differential peaks highlighted in gray. Spont. res., spontaneously resolved infection; tx, treatment.

in mediating continued impairment of HCV-specific responses. Epigenetic scars include super-enhancer elements near critical exhaustion-associated transcription factors such as TOX and HIF-1α, which may provide positive feedback to maintain the state of exhaustion. Consistent with this, we observe persistent high expression of genes neighboring not just scarred but also reversed ChARs after DAA therapy. Further study is required to assess whether the epigenetic scars are maintained indefinitely and how their persistence could be impacted by shifts in subpopulations of exhausted T cells.

There are several other limitations to our study. First, the lack of epigenetic remodeling within bystander populations in chronic HCV might not be generalizable to other diseases like HIV. Second, the degree of epigenetic changes may be related to priming or the amount of re-activation experienced by bystander T cells in chronic contexts and therefore, Flu-specific responses—which are often generated early in life—may be relatively shielded. Due to the limited sample size, we are at present unable to resolve whether differences in the amount of epigenetic scarring observed between conserved and escaped HCV-specific responses could be partially driven by epitope-specific differences. Finally, CD8+ T cell populations in the peripheral blood compartment may not perfectly reflect those found in the liver in chronic HCV infection[49]. Nevertheless, our data are consistent with studies showing that chronic TCR signaling is necessary and sufficient to induce molecular, transcriptional and epigenetic changes of exhaustion in human T cells activated in vitro[50]. The critical regulatory impact of retained epigenetic scars may underlie emerging evidence that HCV-specific T cells isolated following cure produce less IFNγ and TNF relative to functional Flu-specific memory cells[21,22]. These findings are also consistent with studies showing limited CD8+ T cell reactivity to HIV antigens[51] and continued demethylation at the PD-1 locus[52] after successful antiretroviral therapy. Thus, continued dysfunction of exhausted CD8+ T cells, even after the removal of antigen, might be mediated by inflexibility at the epigenetic level.

In this study we show that the distinct epigenetic landscape of T cell exhaustion cannot be fully reversed by the cure of chronic viral infection and is instead maintained long-term. In addition to providing greater insight into the regulation of exhausted T cells, these findings have important implications for therapeutic strategies targeting T cell dysfunction. The epigenetic irreversibility of exhausted T cells observed herein is consistent with previous studies showing that checkpoint-blockade immunotherapy does not fundamentally reverse exhaustion-associated epigenetic changes[43,44].

Furthermore, we show that the degree of scarring may be driven by the timing and magnitude of TCR stimulation. The reversal of T cell exhaustion may thus require targeted approaches to modulate the inflexible epigenetic program that mediates dysfunction and restrains the generation of protective memory T cell responses.

Online content

Any methods, additional references, Nature Research reporting summaries, source data, extended data, supplementary information, acknowledgements, peer review information; details of author contributions and competing interests; and statements of data and code availability are available at https://doi.org/10.1038/s41590-021-00979-1.

Received: 19 May 2020; Accepted: 17 June 2021;
Published online: 26 July 2021

References

1. Hashimoto, M. et al. CD8 T cell exhaustion in chronic infection and cancer: opportunities for interventions. *Annu. Rev. Med.* **69**, 301–318 (2018).
2. Wherry, E. J. et al. Molecular signature of CD8$^+$ T cell exhaustion during chronic viral infection. *Immunity* **27**, 670–684 (2007).
3. Doering, T. A. et al. Network analysis reveals centrally connected genes and pathways involved in CD8$^+$ T cell exhaustion versus memory. *Immunity* **37**, 1130–1144 (2012).
4. Sen, D. R. et al. The epigenetic landscape of T cell exhaustion. *Science* **354**, 1165–1169 (2016).
5. Gallimore, A. et al. Induction and exhaustion of lymphocytic choriomeningitis virus–specific cytotoxic T lymphocytes visualized using soluble tetrameric major histocompatibility complex class I–peptide complexes. *J. Exp. Med.* **187**, 1383–1393 (1998).
6. Zajac, A. J. et al. Viral immune evasion due to persistence of activated T cells without effector function. *J. Exp. Med.* **188**, 2205–2213 (1998).
7. Wherry, E. J., Blattman, J. N., Murali-Krishna, K., van der Most, R. & Ahmed, R. Viral persistence alters CD8 T-cell immunodominance and tissue distribution and results in distinct stages of functional impairment. *J. Virol.* **77**, 4911–4927 (2003).
8. Blackburn, S. D. et al. Coregulation of CD8$^+$ T cell exhaustion by multiple inhibitory receptors during chronic viral infection. *Nat. Immunol.* **10**, 29–37 (2009).
9. Day, C. L. et al. PD-1 expression on HIV-specific T cells is associated with T-cell exhaustion and disease progression. *Nature* **443**, 350–354 (2006).
10. Gruener, N. H. et al. Sustained dysfunction of antiviral CD8$^+$ T lymphocytes after infection with hepatitis C virus. *J. Virol.* **75**, 5550–5558 (2001).
11. Wedemeyer, H. et al. Impaired effector function of hepatitis C virus-specific CD8$^+$ T cells in chronic hepatitis C virus infection. *J. Immunol.* **169**, 3447–3458 (2002).
12. Radziewicz, H. et al. Liver-infiltrating lymphocytes in chronic human hepatitis C virus infection display an exhausted phenotype with high levels of PD-1 and low levels of CD127 expression. *J. Virol.* **81**, 2545–2553 (2007).
13. Wolski, D. et al. Early transcriptional divergence marks virus-specific primary human CD8$^+$ T cells in chronic versus acute infection. *Immunity* **47**, 648–663 (2017).
14. Micallef, J. M., Kaldor, J. M. & Dore, G. J. Spontaneous viral clearance following acute hepatitis C infection: a systematic review of longitudinal studies. *J. Viral Hepat.* **13**, 34–41 (2006).
15. Cox, A. L. et al. Cellular immune selection with hepatitis C virus persistence in humans. *J. Exp. Med.* **201**, 1741–1752 (2005).
16. Kuntzen, T. et al. Viral sequence evolution in acute hepatitis C virus infection. *J. Virol.* **81**, 11658–11668 (2007).
17. Rutebemberwa, A. et al. High-programmed death-1 levels on hepatitis C virus-specific T cells during acute infection are associated with viral persistence and require preservation of cognate antigen during chronic infection. *J. Immunol.* **181**, 8215–8225 (2008).
18. Feld, J. J. et al. Treatment of HCV with ABT-450/r-ombitasvir and dasabuvir with ribavirin. *N. Engl. J. Med.* **370**, 1594–1603 (2014).
19. Ferenci, P. et al. ABT-450/r-ombitasvir and dasabuvir with or without ribavirin for HCV. *N. Engl. J. Med.* **370**, 1983–1992 (2014).
20. Baumert, T. F., Berg, T., Lim, J. K. & Nelson, D. R. Status of direct-acting antiviral therapy for hepatitis C virus infection and remaining challenges. *Gastroenterology* **156**, 431–445 (2019).
21. Wieland, D. et al. TCF1$^+$ hepatitis C virus-specific CD8$^+$ T cells are maintained after cessation of chronic antigen stimulation. *Nat. Commun.* **8**, 15050 (2017).
22. Hensel, N. et al. Memory-like HCV-specific CD8$^+$ T cells retain a molecular scar after cure of chronic HCV infection. *Nat. Immunol.* **22**, 229–239 (2021).
23. Joshi, N. S. et al. Inflammation directs memory precursor and short-lived effector CD8$^+$ T cell fates via the graded expression of T-bet transcription factor. *Immunity* **27**, 281–295 (2007).
24. Martinez, G. J. et al. The transcription factor NFAT promotes exhaustion of activated CD8$^+$ T cells. *Immunity* **42**, 265–278 (2015).
25. Gate, R. E. et al. Genetic determinants of co-accessible chromatin regions in activated T cells across humans. *Nat. Genet.* **50**, 1140–1150 (2018).
26. Rasool, S. T. et al. Increased level of IL-32 during human immunodeficiency virus infection suppresses HIV replication. *Immunol. Lett.* **117**, 161–167 (2008).
27. El-Far, M. et al. Proinflammatory isoforms of IL-32 as novel and robust biomarkers for control failure in HIV-infected slow progressors. *Sci. Rep.* **6**, 22902 (2016).
28. Nguyen, S. et al. Elite control of HIV is associated with distinct functional and transcriptional signatures in lymphoid tissue CD8$^+$ T cells. *Sci. Transl. Med.* https://doi.org/10.1126/scitranslmed.aax4077 (2019).
29. Zaidan, S. M. et al. Upregulation of IL-32 isoforms in virologically suppressed HIV-infected individuals: potential role in persistent inflammation and transcription from stable HIV-1 reservoirs. *J. Acquir. Immune Defic. Syndr.* **82**, 503–513 (2019).
30. Chinnaswamy, S. Genetic variants at the IFNL3 locus and their association with hepatitis C virus infections reveal novel insights into host-virus interactions. *J. Interferon Cytokine Res.* **34**, 479–497 (2014).
31. Monteleone, K. et al. Interleukin-32 isoforms: expression, interaction with interferon-regulated genes and clinical significance in chronically HIV-1-infected patients. *Med. Microbiol. Immunol.* **203**, 207–216 (2014).
32. Wherry, E. J. & Kurachi, M. Molecular and cellular insights into T cell exhaustion. *Nat. Rev. Immunol.* **15**, 486–499 (2015).
33. Whyte, W. A. et al. Master transcription factors and mediator establish super-enhancers at key cell identity genes. *Cell* **153**, 307–319 (2013).
34. Chipumuro, E. et al. CDK7 inhibition suppresses super-enhancer-linked oncogenic transcription in MYCN-driven cancer. *Cell* **159**, 1126–1139 (2014).
35. Adam, R. C. et al. Pioneer factors govern super-enhancer dynamics in stem cell plasticity and lineage choice. *Nature* **521**, 366–370 (2015).
36. Vahedi, G. et al. Super-enhancers delineate disease-associated regulatory nodes in T cells. *Nature* **520**, 558–562 (2015).
37. Ma, S. et al. Chromatin potential identified by shared single-cell profiling of RNA and chromatin. *Cell* **183**, 1103–1116 (2020).
38. Khan, O. et al. TOX transcriptionally and epigenetically programs CD8$^+$ T cell exhaustion. *Nature* **571**, 211–218 (2019).
39. Scott, A. C. et al. TOX is a critical regulator of tumour-specific T cell differentiation. *Nature* **571**, 270–274 (2019).
40. Alfei, F. et al. TOX reinforces the phenotype and longevity of exhausted T cells in chronic viral infection. *Nature* **571**, 265–269 (2019).
41. Urbani, S. et al. PD-1 expression in acute hepatitis C virus (HCV) infection is associated with HCV-specific CD8 exhaustion. *J. Virol.* **80**, 11398–11403 (2006).
42. Bengsch, B. et al. Coexpression of PD-1, 2B4, CD160 and KLRG1 on exhausted HCV-specific CD8$^+$ T cells is linked to antigen recognition and T cell differentiation. *PLoS Pathog.* **6**, e1000947 (2010).
43. Pauken, K. E. et al. Epigenetic stability of exhausted T cells limits durability of reinvigoration by PD-1 blockade. *Science* **354**, 1160–1165 (2016).
44. Miller, B. C. et al. Subsets of exhausted CD8$^+$ T cells differentially mediate tumor control and respond to checkpoint blockade. *Nat. Immunol.* **20**, 326–336 (2019).
45. Alatrakchi, N. et al. Hepatitis C virus (HCV)-specific CD8$^+$ cells produce transforming growth factor β that can suppress HCV-specific T-cell responses. *J. Virol.* **81**, 5882–5892 (2007).
46. Brooks, D. G. et al. Interleukin-10 determines viral clearance or persistence in vivo. *Nat. Med.* **12**, 1301–1309 (2006).
47. Ejrnaes, M. et al. Resolution of a chronic viral infection after interleukin-10 receptor blockade. *J. Exp. Med.* **203**, 2461–2472 (2006).
48. Tinoco, R., Alcalde, V., Yang, Y., Sauer, K. & Zuniga, E. I. Cell-intrinsic transforming growth factor-β signaling mediates virus-specific CD8$^+$ T cell deletion and viral persistence in vivo. *Immunity* **31**, 145–157 (2009).
49. Kroy, D. C. et al. Liver environment and HCV replication affect human T-cell phenotype and expression of inhibitory receptors. *Gastroenterology* **146**, 550–561 (2014).
50. Lynn, R. C. et al. c-Jun overexpression in CAR T cells induces exhaustion resistance. *Nature* **576**, 293–300 (2019).
51. Rutishauser, R. L. et al. Early and delayed antiretroviral therapy results in comparable reductions in CD8$^+$ T cell exhaustion marker expression. *AIDS Res. Hum. Retroviruses* **33**, 658–667 (2017).
52. Youngblood, B. et al. Cutting edge: prolonged exposure to HIV reinforces a poised epigenetic program for PD-1 expression in virus-specific CD8 T cells. *J. Immunol.* **191**, 540–544 (2013).

Methods

Study participants. For the HCV cohort (Supplementary Table 1), all patients were enrolled in an open label phase 3 clinical trial of paritaprevir/ritonavir, ombitasvir, dasabuvir and ribavirin for genotype 1a HCV infection designed to evaluate the effect of successful antiviral therapy on innate and adaptive immune responses (NCT02476617). The trial was approved by the Massachusetts General Hospital Institutional Review Board.

The participants of the trial were confirmed to be chronically infected with HCV genotype 1a infection, based on viral load, and screened for specific HLA alleles. To reduce the impact of sources of variability or bias, individuals who had tested positive for co-infections, such as HIV or hepatitis B, or resolved a previous infection on their own were excluded.

The trial participants were treated with a combination of paritaprevir/ritonavir, ombitasvir, dasabuvir and ribavirin for 12 weeks. Only patients with HCV RNA levels below the lower limit of quantification 12 weeks after the last dose of the study drug were included for further analysis. All of the included patients were followed for at least one year following treatment. Informed consent was given by all participants under protocols approved by the Massachusetts General Hospital Institutional Review Board.

Blood samples were collected from six patients via leukapheresis at two or three time points representing pre-treatment, 12 weeks post treatment and long-term follow-up (60–80 weeks post treatment). Peripheral blood mononuclear cells were extracted by Ficoll–Paque (GE Healthcare Life Sciences) density gradient centrifugation and frozen down for further processing. A small aliquot of the sample was reserved and analyzed by flow cytometry to identify the virus-specific $CD8^+$ T cell responses using the appropriate HLA class I multimers. The circulating HCV virus was then sequenced and compared with known epitopes that had elicited T cell responses. If the viral repertoire of the donor fully matched the epitope peptide sequence, that corresponding T cell response was considered conserved. If the viral repertoire of the donor diverged from the epitope peptide sequence, the ability of the new variant peptides to re-stimulate HCV-specific T cells was assayed. Only T cell responses that had no or minimal (less than 10% of the original sequence) responsiveness were classified as HCV Esc. Partially escaped T cell responses were excluded from this study.

For the HIV cohort (Supplementary Table 4), all patients were enrolled in either the SPARTAC ('Short Pulse Anti-Retroviral Therapy at Seroconversion') or HEATHER ('HIV Reservoir targeting with Early Antiretroviral Therapy') trials. The SPARTAC trial (EudraCT number: 2004-000446-20) was approved by the following authorities: Medicines and Healthcare products Regulatory Agency (UK), Ministry of Health (Brazil), Irish Medicines Board (Ireland), Medicines Control Council (South Africa) and Uganda National Council for Science and Technology (Uganda). It was also approved by the following ethics committees in the participating countries: Central London Research Ethics Committee (UK); Hospital Universitário Clementino Fraga Filho Ethics in Research Committee (Brazil); Clinical Research and Ethics Committee of Hospital Clinic in the province of Barcelona (Spain); Adelaide and Meath Hospital Research Ethics Committee (Ireland); University of Witwatersrand Human Research Ethics Committee, University of Kwazulu-Natal Research Ethics Committee and University of Cape Town Research Ethics Committee (South Africa); Uganda Virus Research Institute Science and Ethics Committee (Uganda); Prince Charles Hospital Human Research Ethics Committee and St Vincent's Hospital Human Research Ethics Committee (Australia); and National Institute for Infectious Diseases Lazzaro Spallanzani, Institute Hospital and the Medical Research Ethics Committee, and the ethical committee of the Central Foundation of San Raffaele, MonteTabor (Italy). The HEATHER trial (REC reference: 14/WM/1104) was approved by the West Midlands–South Birmingham Research Ethics Committee. Informed consent was given by all participants.

The full inclusion criteria and details of these trials are published elsewhere[53,54] and were similar in terms of inclusion criteria and demographics. Briefly, the inclusion criteria were: positive HIV-1 antibody test within 6 months of a negative HIV-1 antibody test, HIV-1-antibody negative with positive PCR (or positive p24 antigen or detectable viral load), recent incident assay test algorithm (RITA) assay result consistent with recent infection, equivocal HIV-1 antibody test supported by a repeat test within 2 weeks showing a rising optical density and clinical manifestations of symptomatic HIV seroconversion illness supported by antigen positivity. Peripheral blood mononuclear cells were collected at each study visit and cryopreserved, as previously described. All samples were collected before the initiation of highly active antiretroviral therapy to enable an unbiased comparison to the HCV cohort before treatment.

Cell isolation and cell sorting. Peripheral blood mononuclear cells from patients with HCV were thawed rapidly in warm T cell culture medium (RPMI medium supplemented with 10% fetal bovine serum) and counted. $CD8^+$ T cells were enriched using a MACS CD8 negative selection kit (Miltenyi). After enrichment, the cells were stained for 15 min at 4 °C using fluorochrome-conjugated multimers for HCV A*02:01 NS3 1073 CINGVCWTV (Immudex), influenza A*02:01 MP GILGFVFTL (Immudex) and other appropriate HCV multimers representing escaped viral epitopes (ProImmune). When required, unlabeled multimers were conjugated to allophycocyanin by staining with Pro5 Fluorotags (ProImmune) as per the manufacturer's protocol.

Multimer-positive cells were enriched using MACS anti-phycoerythrin, anti-allophycocyanin and anti-fluorescein isothiocyanate positive selection kits (Miltenyi). The cells were then stained for the cell surface markers and sorted on a FACSAria cell sorter (BD Biosciences) using the FACSDIVA software (v.8.0.1). The following antibodies (all from BioLegend) and stains were used: anti-CD45RA (HI100; 1:50), anti-CCR7 (G043H7; 1:50), anti-CD3 (OKT3; 1:50), anti-CD39 (A1; 1:20), anti-PD-1 (EH12.2H7; 1:20), anti-CD8a (SK1; 1:50), anti-CD95 (DX2; 1:20) and Near-IR live/dead (Invitrogen; 1:1,000). The cell sorting strategy has been summarized in Extended Data Fig. 1. We used three additional markers for sorting bulk naive and bulk effector-memory T cells (CCR7, CD45RA and CD95) as follows: naive, live $CD3^+CD8^+$multimer$^-$$CCR7^+CD45RA^-$; and effector memory, live $CD3^+CD8^+$multimer$^-$$CCR7^-CD45RA^-$). Cells were stained with the markers CD39 and PD-1 only to enable subsequent analysis of protein expression and were not used for any sort gates. All of the flow data were analyzed using FlowJo version 10.4.1. A maximum of 80,000 cells were sorted into PBS supplemented with 10% fetal bovine serum for subsequent ATAC-seq library generation.

For the HIV cohort, the following fluorochrome-conjugated multimers from ImmunAware were used: HIV A*02:01 RLRPGGKKK, HIV B*07:02 GPGHKARVL, HIV B*57:01 KAFSPEVIPMF and HIV B*53:01 YPLTFGWCF. Cell isolation and processing were performed as previously described but without secondary multimer enrichment.

ATAC-seq library generation. ATAC-seq libraries were generated as previously described. Briefly, cell counts from the sorter were adjusted by assuming 65–70% cell loss. The sorted cells were pelleted for 10 min at 400*g* and incubated in 5–50 µl of Tn5 reaction mix (2×TD buffer, Tn5 enzyme and 2% digitonin in nuclease-free water) for 30 min at 37 °C. DNA was purified using a Qiagen MinElute reaction cleanup kit and PCR was used to add dual-indexed barcodes (Illumina). Post-PCR cleanup was done using Agencourt AMPure XP beads (Beckman Coulter) and the ATAC-seq library quality was verified using Tapestation analysis. Patient samples across multiple time points were pooled for sequencing whenever possible to minimize batch effects. The samples were sequenced on an Illumina NextSeq500 sequencer using paired-end 37-bp reads.

Data processing and quality control. Sequencing reads were demultiplexed into fastq files using bcl2fastq (v2.19.1.403). Quality trimming and primer removal from the raw fastq files were performed using Trimmomatic (v0.36) using the following parameters: LEADING:15 TRAILING:15 SLIDINGWINDOW:4:15 and MINLEN:36. Quality control of the sequencing reads was performed before and after quality trimming using the FastQC software (Babraham Bioinformatics). The trimmed reads were aligned to hg19 using Bowtie2 (v2.2.9) using a maximum insert size of 1,000. The aligned bam files were sorted, duplicates were marked and reads mapping to the blacklist[55] region were removed using PICARD. The aligned reads were shifted +4 bp or −5 bp, as appropriate. All of the samples were assessed for library quality according to the ENCODE guidelines (https://www.encodeproject.org/atac-seq/). Briefly, the fraction of reads in the called peak regions (FRiP score) as well as the transcriptional-start-site enrichment was calculated as previously described. In addition, the concordance of each biological condition was assessed by the average Pearson correlation across all pairwise combinations.

Peak universe generation and differential accessibility analysis. For consensus peak generation, biological replicate samples ($n = 6$ patients) were downsampled to the lowest read count among the replicates separately for each of 12 biological conditions (naive, Flu tet^+, HCV tet^+ and HCV Esc tet^+; three time points each). Downsampled bams for each biological replicate were then merged using Samtools v1.3.1. Peak-calling was performed for each biological condition using MACS (v2.1.1) on merged bam files with a *q*-value threshold of 0.001. Consensus peaks from all biological conditions were then merged to create a single HCV peak universe of 128,327 regions. Cut sites were extracted from each biological replicate and the number of cuts within each peak region was quantified (BEDtools v2.26.0) to generate a raw counts matrix. DESeq2 (v1.18.1) was used to normalize the counts matrix and perform differential accessibility analysis between all of the relevant comparisons. For any given comparison, an FDR cutoff of 0.05 was used to determine the differential ChARs.

Comparative analysis of chromatin accessibility from the LCMV mouse model. Orthologous mouse ChARs (mm10) were mapped to the human genome (hg19) as described[4]. As the mapping algorithm requires input regions in mm10, the UCSC liftover tool was applied to ChARs to transfer them onto mm10 from mm9. All of the mouse peaks partitioned into three categories based on previously published clustering: peaks found in the naive cluster a (mouse naive), peaks found in the acute day 27 cluster c (mouse memory) and peaks found in the chronic day 27 cluster e (mouse exhausted). The hypergeometric fold enrichment was then calculated separately for the three categories of the mouse orthologous peaks (naive, memory and exhaustion) for each set of consensus peaks in the HCV dataset.

Enhancer classification. For the identification of scarred, reversed and gained regions, we first identified all ChARs that were significantly more accessible in HCV tet^+ cells compared with Flu tet^+ cells before treatment ($n = 21,490$; FDR < 0.05).

Of these, all ChARs that became significantly less accessible in the HCV tet$^+$ cells following treatment compared with the pre-treatment HCV tet$^+$ cells were denoted as reversed ($n=5,203$; FDR <0.05). In contrast, all of the ChARs that were unchanged in the HCV tet$^+$ cells before and after treatment (FDR >0.05 and absolute fold change <1.5) were termed scarred ($n=5,769$). Finally, ChARs that became significantly more accessible in the post-treatment HCV tet$^+$ cells compared with pre-treatment HCV tet$^+$ cells were denoted as gained ($n=17,739$; FDR <0.05). These analyses, as summarized in Figs. 1–3, were conducted only on conserved HCV responses relative to Flu-specific and naive T cells. Escaped responses were always analyzed separately and are denoted as HCV Esc in the figures and text.

Pathway and motif enrichment. Gene-to-peak associations were determined using the GREAT software package (v3.0.0, http://bejerano.stanford.edu/great/public/html/) with default settings. GREAT was also used to determine the gene-set enrichment, with default settings and the binomial test to measure significance. Motif enrichment analysis was performed using HOMER (v3.0) with default settings.

SNP overlap analysis. All GWAS SNPs in the NHGRI catalog (https://www.ebi.ac.uk/gwas/) annotated as 'AIDS', 'Chronic hepatitis B virus infection', 'Hepatitis B virus infection', 'Hepatitis C virus infection', 'HIV infection' or 'HIV-1 infection' were defined as being chronic-infection-related. A detailed summary of all chronic-infection-related SNPs along with the associated metadata are provided in Supplementary Table 3. Hypergeometric tests were performed to quantify the overlap of enhancers with all GWAS SNPS and chronic-infection-related SNPs.

Inference and validation of super-enhancer-associated genes. Super-enhancers are composed of multiple constituent enhancer segments encompassing large chromatin domains that are broadly marked by H3K27ac histone mark and/or Mediator binding[33,35]. Given that ATAC-seq identifies smaller, more punctate regions of chromatin accessibility, we reasoned that counting the number of regulatory units near a given gene would allow us to approximate broad stretches of H3K27ac accumulation in super-enhancers[37]. Based on this principle, super-enhancers were identified by counting individual putative enhancers per gene in each sample. Specifically, the online tool GREAT (see the 'Pathway and motif enrichment' section) was used to assign each ChAR to the nearby gene(s). The number of regions per gene was then calculated and the resultant list was ranked from highest to lowest. The list of ranked genes could then be plotted against the total number of regions to generate a characteristic elbow plot. As observed in the original definition of super-enhancers[33], this gene-centric approach also revealed a clear point in the distribution where the number of enhancers per gene increased rapidly. The x and y axes were then scaled from zero to one and the inflection point in the curve was determined using the findElbow tool in the ChemoSpecMarkeR package (B. A. Hanson). All genes with a higher number of regions than the inflection point were defined as super-enhancer-associated. This method can be used to call super-enhancer-associated genes from any set of ChARs, ranging from the whole universe to subsets of regions such as scarred or reversed.

Note that this analysis directly identifies a set of genes associated with super-enhancer-like loci rather than identifying chromatin regions themselves, thereby allowing for less ambiguity in assigning super-enhancers to genes. However, the constituent enhancers of a putative super-enhancer can still be identified by inspecting the regions that are assigned to a super-enhancer-associated gene.

The performance of this method was tested by its ability to predict super-enhancer-associated genes as defined by the H3K27ac gold-standard. For consistency, H3K27ac-based super-enhancers were assigned to genes using the GREAT tool. Eight human tissues were chosen based on the availability of matched ATAC-seq, H3K27ac ChIP-seq and RNA-sequencing datasets. Lists of H3K27ac-based super-enhancers for each tissue were obtained from dbSUPER (https://asntech.org/dbsuper/) and associated to genes using the GREAT tool for internal consistency. Paired ATAC-seq data for each tissue were obtained from ENCODE and super-enhancer-associated gene identification was performed in the space of all regions as previously described. Genes associated with H3K27ac-based super-enhancers were used as the 'true-positives' to generate receiver-operating-characteristic curves for the predictive power of ATAC-based super-enhancer inference.

Statistics and data visualization. Statistical analysis of differential chromatin accessibility tests was performed using DESeq2, and FDR correction was performed using the Benjamini–Hochberg method in R 3.6.1. Two-group two-sided Mann–Whitney U tests were run to compare differences in the levels of mRNA expression of neighboring genes in Figs. 1 and 5. The statistical significance of gene-ontology-term enrichments and motif enrichments were calculated with two-sided hypergeometric tests. The statistical significance of the ChARs overlapping GWAS SNPs, HIV-specific regions or mouse orthologous ChARs was determined using two-sided hypergeometric tests. P values and q-values that were <0.05 were considered to indicate a significant difference. Asterisks were used to indicate significance as follows: $^*P<0.05$, $^{**}P<0.01$, $^{***}P<0.001$ and $^{****}P<0.0001$.

ATAC-seq tracks were visualized using Integrative Genomics Viewer (v2.3.77). GENE-E (v3.0.215) was used for heatmap visualization and similarity matrix calculations (Pearson). The PCA was done using R (v3.3.1) in RStudio (v1.1.453). Volcano plots were generated using GraphPad Prism 7. All boxplots depict the median, with the box representing the middle 50th percentile and the whiskers representing the range.

Reporting Summary. Further information on research design is available in the Nature Research Reporting Summary linked to this article.

Data availability

All sequencing data from this study will be made publicly available through the National Center for Biotechnology Information (NCBI) Gene Expression Omnibus (GEO; https://www.ncbi.nlm.nih.gov/geo/) and/or NCBI database of Genotypes and Phenotypes (dbGaP; https://www.ncbi.nlm.nih.gov/gap/). All other relevant data are available from the corresponding authors on request.

References

53. The SPARTAC Trial Investigators. Short-course antiretroviral therapy in primary HIV infection. *N. Engl. J. Med.* **368**, 207–217 (2013).
54. Hoffmann, M. et al. Exhaustion of activated CD8 T cells predicts disease progression in primary HIV-1 infection. *PLoS Pathog.* **12**, e1005661 (2016).
55. Amemiya, H. M., Kundaje, A. & Boyle, A. P. The ENCODE blacklist: identification of problematic regions of the genome. *Sci. Rep.* **9**, 9354 (2019).

Acknowledgements

We thank the members of the Haining laboratory for their input and the research participants for their participation. This work was supported by NIH grant no. U19 AI086230 and funding from the Parker Institute for Cancer Immunotherapy. S.A.W. was supported by NIH grant nos. T32 GM007753 and T32 CA207021; R.T.C. was supported by AI136715 and the MGH Research Scholars Program. We also thank the Center for Virology and Vaccine Research Flow Cytometry Core at Beth Israel Deaconess Medical Center for their assistance.

Author contributions

D.R.S. and W.N.H. conceived the study and designed the experiments. D.R.S., K.B.Y., G.E.M., U.G., R.A.A., D.E.C. and S.A.W. performed experiments and/or data analysis. P.T., D.W., D.C.T., R.T.C., T.M.A., A.Y.K. and G.M.L. contributed to the HCV clinical trial design, patient recruitment, sample processing, viral sequencing studies and/or transcriptional analysis. G.E.M., S.F., J. Frater. and J. Fox contributed to the HIV clinical trial design, patient recruitment and/or sample processing. D.R.S. and W.N.H. wrote the manuscript; all authors reviewed and edited the manuscript.

Competing interests

AbbVie sponsored the clinical trial (NCT02476617) and gave input to the trial design as well as the clinical and biological sample collection schedule. W.N.H. is an employee of Merck and Company and holds equity in Tango Therapeutics and Arsenal Biosciences. The other authors declare no competing interests.

Additional information

Extended data is available for this paper at https://doi.org/10.1038/s41590-021-00979-1.

Supplementary information The online version contains supplementary material available at https://doi.org/10.1038/s41590-021-00979-1.

Correspondence and requests for materials should be addressed to W.N.H. or D.R.S.

Peer review information *Nature Immunology* thanks Hazem Ghoneim, Barbara Rehermann and the other, anonymous, reviewer(s) for their contribution to the peer review of this work. Peer reviewer reports are available. Zoltan Fehervari was the primary editor on this article and managed its editorial process and peer review in collaboration with the rest of the editorial team.

Reprints and permissions information is available at www.nature.com/reprints.

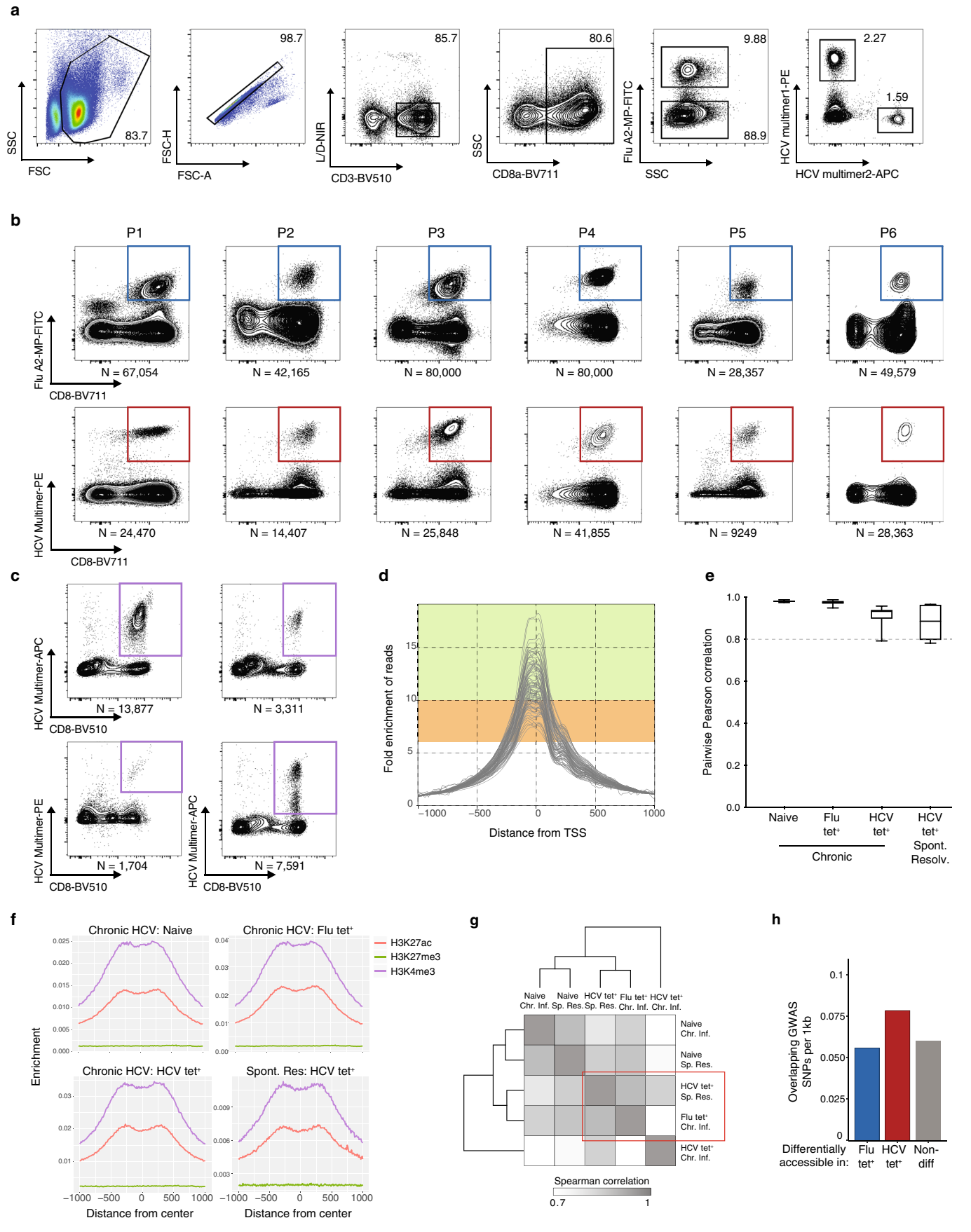

Extended Data Fig. 1 | See next page for caption.

Extended Data Fig. 1 | Isolation and chromatin accessibility profiling of Flu and HCV multimer$^+$ CD8$^+$ T cells in HCV infection. a, Representative flow cytometry sorting strategy for Flu and HCV multimer+ CD8+ T cells. **b**, Recovered numbers of Flu (top) and HCV (bottom) multimer+ cells for each donor during chronic HCV infection. **c**, Recovered numbers of HCV multimer+ cells for each donor during resolved HCV infection. **d**, Combined ATAC signal across all TSSs for each biological condition from each donor. Green and range bands indicate ranges for ideal and acceptable values, respectively, for TSS enrichment per ENCODE standards. **e**, Boxplots of pairwise Pearson correlations for data from individual donors within each biological condition. Center, median; box limits, first and third percentiles; whiskers, min and max. N = 6 donors. **f**, Combined ATAC signal across all H3K27ac peaks (red), H3K27me3 (green) and H3K4me3 (purple). Histone mark peaks were determined from the following samples on ENCODE: ENCFF653OGM - H3K27ac, ENCFF285FID - H3K4me3, ENCFF367HSC - H3K27me3. **g**, Clustered similarity matrix between the indicated biological conditions in the chronically-infected and spontaneously resolved cohort. **h**, Density of overlapping GWAS SNPs per 1000 bp in Flu-specific, HCV-specific or non-differential ChARs.

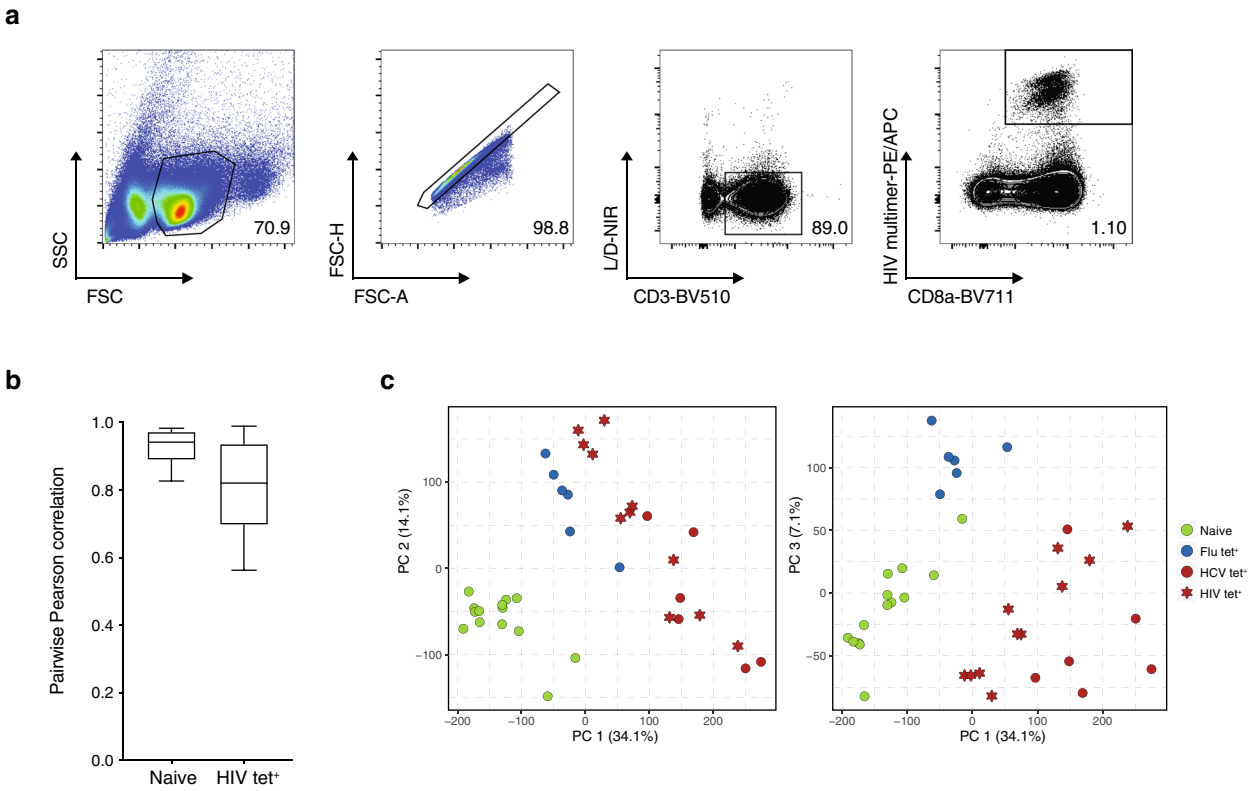

Extended Data Fig. 2 | Isolation and chromatin accessibility profiling of HIV multimer$^+$ CD8$^+$ T cells in HIV infection. a, Representative flow cytometry sorting strategy for HIV multimer+ CD8+ T cells. **b**, Boxplots of pairwise Pearson correlations for data from individual donors within each biological condition. Center, median; box limits, first and third percentiles; whiskers, min and max. N = 11 donors. **c**, Combined principal component analysis of naïve, HIV-, HCV- and Flu- specific CD8+ T cells from the HIV and HCV cohorts.

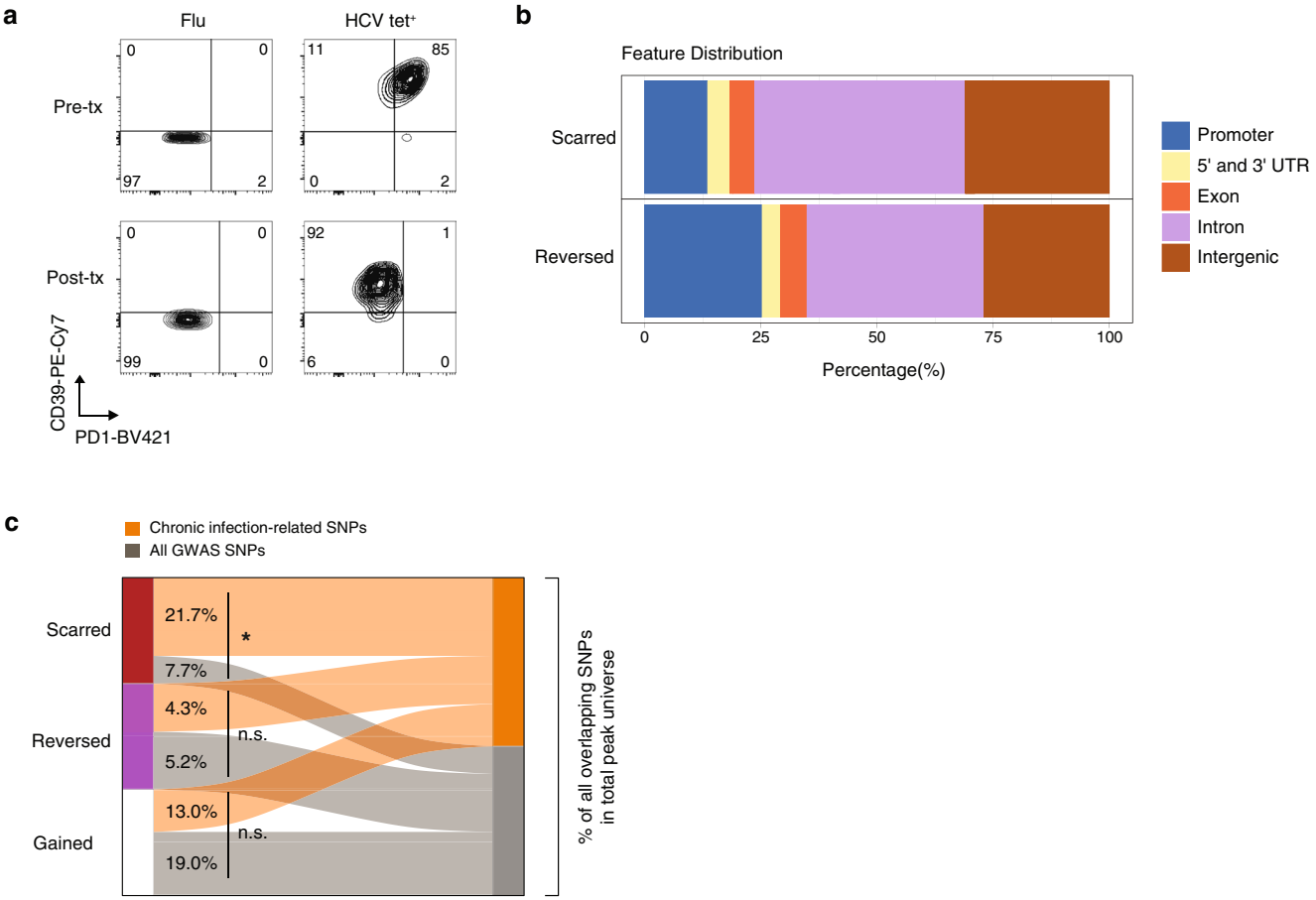

Extended Data Fig. 3 | Features of HCV-specific CD8⁺ T cells before and after DAA therapy. a, PD-1 and CD39 staining on tetramer populations before (top) and after (bottom) DAA therapy. **b**, Partitioning of scarred and reversed regions into those overlapping promoters, UTRs, exons, introns and intergenic areas as indicated. **c**, Classification of SNPs falling within scarred, reversed or gained ChARs. SNPs that were subcategorized into those associated with chronic viral infection are summarized in Supplementary Table 3.

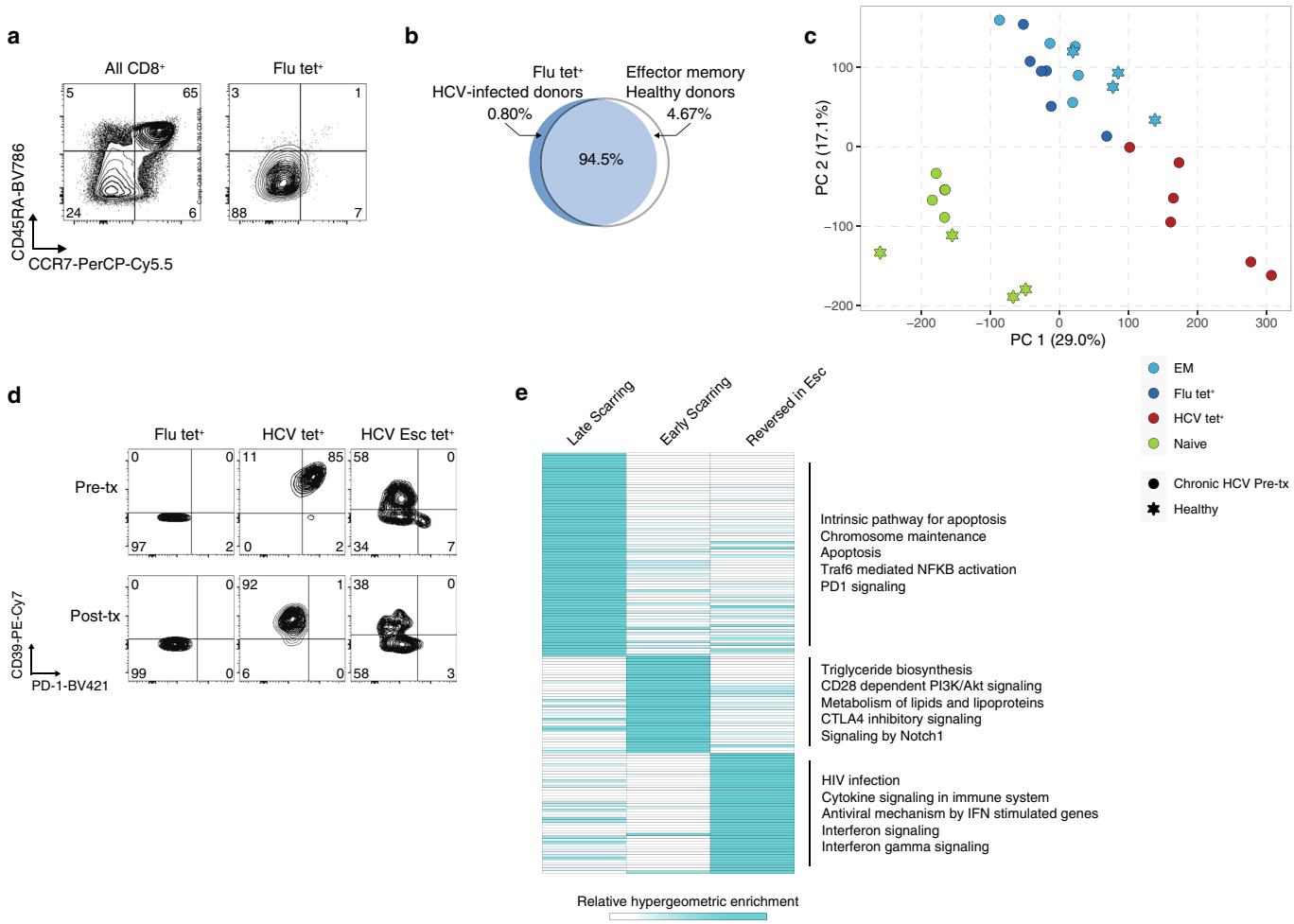

Extended Data Fig. 4 | Minimal impact of the inflammatory milieu on chromatin accessibility within bystander populations in chronic HCV. a, CCR7 and CD45RA staining on all CD8+ T cells (left) and Flu-specific T cells (right). **b**, Venn diagram of ChAR overlap in Flu tet+ cells (bottom) from HCV-infected donors and healthy donors. **c**, PD-1 and CD39 staining on tetramer populations before (top) and after (bottom) DAA therapy. **d**, Combined principal component analysis of naïve, effector memory, HCV-, and Flu- specific CD8+ T cells from the healthy and HCV cohorts. **e**, Heatmap showing pathway enrichment (rows) within clustered ChARs from Fig. 4g (columns).

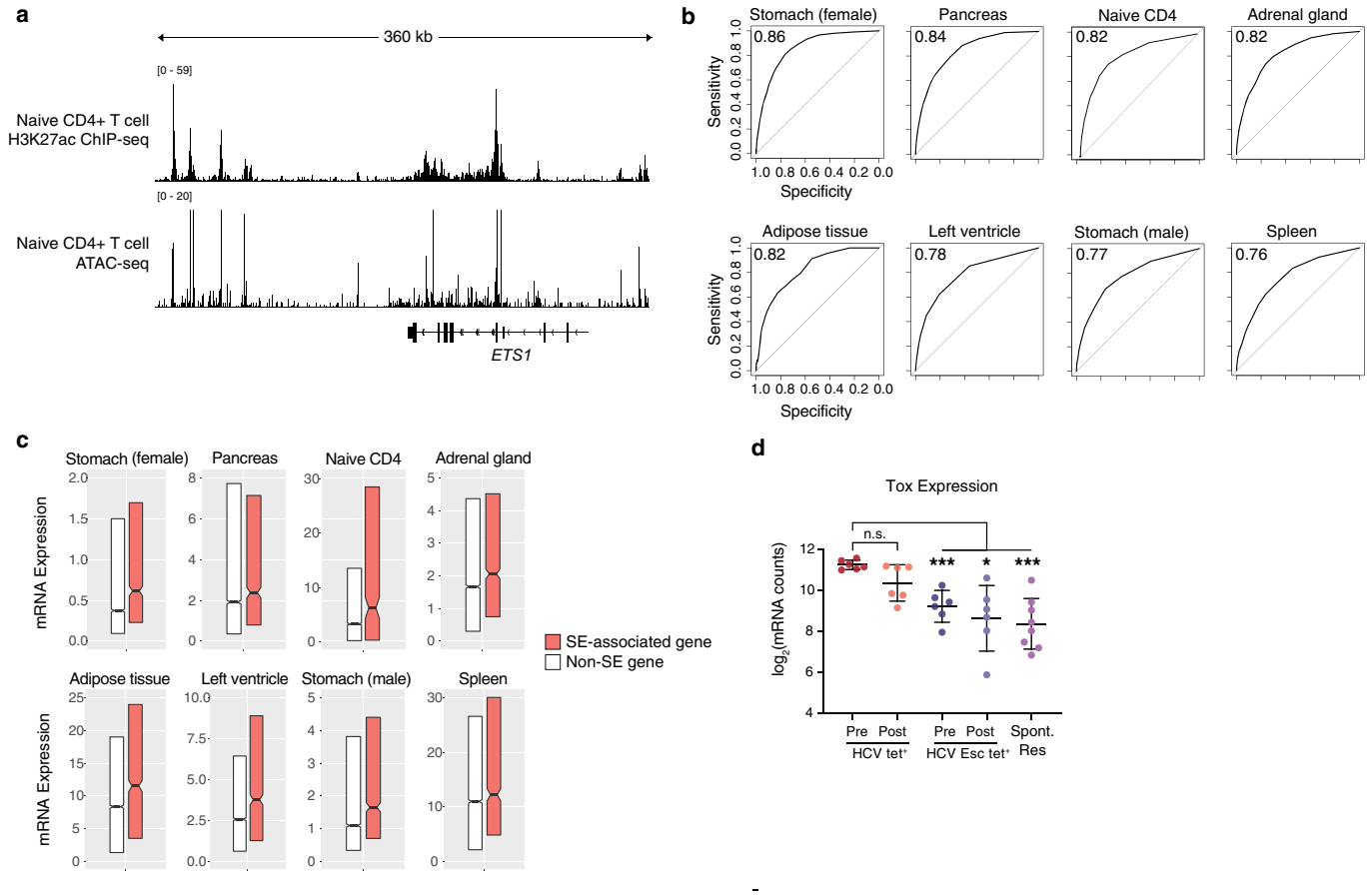

Extended Data Fig. 5 | Validation of ATAC-seq-based super-enhancer inference across multiple datasets. a, H3K27ac ChIP-seq signal (top) and ATAC-seq signal (bottom) at the ETS1 gene locus. **b**, ROC plots of varying cutoff for ATAC-based ranking of super-enhancer to predict bona fide super-enhancers defined using matched tissue-specific H3K27ac ChIP-seq. **c**, Boxplots of tissue-specific mRNA expression, partitioned by genes with or without an associated super-enhancer. Center, median; box limits, first and third percentiles. **d**, Tox mRNA expression in HCV tetramer populations before and after DAA therapy. Mean ± s.d., two-sided Student's t-test with Welch's correction; *P ≤ 0.05, **P ≤ 0.01, ***P ≤ 0.001. N = 6 donors.

nature research

Corresponding author(s): W. Nicholas Haining, Debattama R. Sen

Last updated by author(s): Apr 10, 2021

Reporting Summary

Nature Research wishes to improve the reproducibility of the work that we publish. This form provides structure for consistency and transparency in reporting. For further information on Nature Research policies, see our Editorial Policies and the Editorial Policy Checklist.

Statistics

For all statistical analyses, confirm that the following items are present in the figure legend, table legend, main text, or Methods section.

n/a	Confirmed
☐	☒ The exact sample size (*n*) for each experimental group/condition, given as a discrete number and unit of measurement
☐	☒ A statement on whether measurements were taken from distinct samples or whether the same sample was measured repeatedly
☐	☒ The statistical test(s) used AND whether they are one- or two-sided *Only common tests should be described solely by name; describe more complex techniques in the Methods section.*
☒	☐ A description of all covariates tested
☐	☒ A description of any assumptions or corrections, such as tests of normality and adjustment for multiple comparisons
☐	☒ A full description of the statistical parameters including central tendency (e.g. means) or other basic estimates (e.g. regression coefficient) AND variation (e.g. standard deviation) or associated estimates of uncertainty (e.g. confidence intervals)
☐	☒ For null hypothesis testing, the test statistic (e.g. *F*, *t*, *r*) with confidence intervals, effect sizes, degrees of freedom and *P* value noted *Give P values as exact values whenever suitable.*
☒	☐ For Bayesian analysis, information on the choice of priors and Markov chain Monte Carlo settings
☒	☐ For hierarchical and complex designs, identification of the appropriate level for tests and full reporting of outcomes
☒	☐ Estimates of effect sizes (e.g. Cohen's *d*, Pearson's *r*), indicating how they were calculated

Our web collection on statistics for biologists contains articles on many of the points above.

Software and code

Policy information about availability of computer code

Data collection	Flow collection was performed using FACSDIVA (BD Pharmingen). All sequencing data was collected on a NextSeq500 (Illumina).
Data analysis	All flow data was analyzed using FlowJo version 10.4.1. All statistical tests were run using Graphpad Prism 7 or R 3.6.1. ATAC-seq analysis was performed using GREAT (3.0.0) and HOMER (4.10). Statistics for ATAC-seq were performed using DESeq2.

For manuscripts utilizing custom algorithms or software that are central to the research but not yet described in published literature, software must be made available to editors and reviewers. We strongly encourage code deposition in a community repository (e.g. GitHub). See the Nature Research guidelines for submitting code & software for further information.

Data

Policy information about availability of data

All manuscripts must include a data availability statement. This statement should provide the following information, where applicable:

- Accession codes, unique identifiers, or web links for publicly available datasets
- A list of figures that have associated raw data
- A description of any restrictions on data availability

All sequencing data (Figures 1-6) will be made available on GEO and/or dbGaP, as appropriate.

Field-specific reporting

Please select the one below that is the best fit for your research. If you are not sure, read the appropriate sections before making your selection.

☒ Life sciences ☐ Behavioural & social sciences ☐ Ecological, evolutionary & environmental sciences

For a reference copy of the document with all sections, see nature.com/documents/nr-reporting-summary-flat.pdf

Life sciences study design

All studies must disclose on these points even when the disclosure is negative.

Sample size	Sample sizes were chosen based on the availability of sufficient biological material to perform required sorting/analysis.
Data exclusions	No data were excluded.
Replication	All attempts to reproduce our findings were successful.
Randomization	All human participants received the same treatment and were profiled equivalently, therefore randomization was not relevant.
Blinding	All human participants received the same treatment and were profiled equivalently, therefore blinding was not relevant. All authors performing data collection and/or analysis were blinded to patient identity.

Reporting for specific materials, systems and methods

We require information from authors about some types of materials, experimental systems and methods used in many studies. Here, indicate whether each material, system or method listed is relevant to your study. If you are not sure if a list item applies to your research, read the appropriate section before selecting a response.

Materials & experimental systems

n/a	Involved in the study
☐	☒ Antibodies
☒	☐ Eukaryotic cell lines
☒	☐ Palaeontology and archaeology
☒	☐ Animals and other organisms
☐	☒ Human research participants
☒	☐ Clinical data
☒	☐ Dual use research of concern

Methods

n/a	Involved in the study
☒	☐ ChIP-seq
☐	☒ Flow cytometry
☒	☐ MRI-based neuroimaging

Antibodies

Antibodies used	Cells were stained for the following cell surface markers from Biolegend: anti–CD45RA (HI100), anti-CCR7 (G043H7), anti-CD3 (OKT3), anti-CD39 (A1), anti-PD-1 (EH12.2H7), anti-CD8a (SK1), anti-CD95 (DX2) and Near-IR Live/Dead (Invitrogen).
Validation	Validation for specificity was confirmed in the data sheets provided by the manufacturer.

Human research participants

Policy information about studies involving human research participants

Population characteristics	All relevant information summarized in Supplementary Tables 1 and 4.
Recruitment	For the HCV cohort (Supplementary Table 1), all patients were enrolled in an open label Phase 3 clinical trial of paritaprevir/ritonavir, ombitasvir, dasabuvir and ribavirin for genotype 1a hepatitis C virus infection designed to evaluate the effect of successful antiviral therapy on innate and adaptive immune responses. For the HIV cohort (Supplementary Table 4), all patients were enrolled in either the SPARTAC ('Short Pulse Anti-Retroviral Therapy at Seroconversion') or HEATHER ('HIV Reservoir targeting with Early Antiretroviral Therapy') trials.
Ethics oversight	HCV trial (NCT02476617) was approved by the Massachusetts General Hospital Institutional Review Board. HIV SPARTAC trial (2004-000446-20) was approved by the following authorities: the Medicines and Healthcare products Regulatory Agency (UK), the Ministry of Health (Brazil), the Irish Medicines Board (Ireland), the Medicines Control Council (South Africa) and the Uganda National Council for Science and Technology (Uganda). HIV HEATHER trial (14/WM/1104) was approved by the West Midlands—South Birmingham Research Ethics Committee.

Note that full information on the approval of the study protocol must also be provided in the manuscript.

Flow Cytometry

Plots

Confirm that:

☒ The axis labels state the marker and fluorochrome used (e.g. CD4-FITC).

☒ The axis scales are clearly visible. Include numbers along axes only for bottom left plot of group (a 'group' is an analysis of identical markers).

☒ All plots are contour plots with outliers or pseudocolor plots.

☒ A numerical value for number of cells or percentage (with statistics) is provided.

Methodology

Sample preparation	Blood samples were collected via leukapheresis or blood draws. Peripheral blood mononuclear cells (PBMCs) were extracted by Ficoll-Paque (GE Healthcare Life Sciences) density gradient centrifugation and frozen down for further processing. PBMCs from patients were thawed rapidly in warm T cell culture medium (RPMI supplemented with 10% FBS) and counted. CD8+ T cells were enriched using MACS CD8 negative selection kit (Miltenyi). After enrichment, cells were stained for 15 minutes at 4°C using appropriate multimers representing viral epitopes. When required, multimer-positive cells were enriched using MACS anti-PE, anti-APC and anti-Fitc positive selection kits (Miltenyi). Cells were then stained for other cell surface markers from Biolegend and sorted on a FACSAria cell sorter (BD Biosciences).
Instrument	BD LSR Fortessa SORP was used to collect data for analysis. BD FACSAria II was used for cell sorting.
Software	All flow data was collected using FACSDIVA (BD Pharmingen) and analyzed using FlowJo version 10.4.1.
Cell population abundance	All sorts had a purity > 95%, checked by post-sort re-sampling.
Gating strategy	Gating strategy summarized in Supplementary Figures 1 and 2, with gates drawn based on single-stain and full-minus-one (FMO) controls.

☒ Tick this box to confirm that a figure exemplifying the gating strategy is provided in the Supplementary Information.